Biomechanics-Based Optimization for Exoskeleton Design

Melanie L. Hook

Thesis submitted to the Faculty of the
Virginia Polytechnic Institute and State University
in partial fulfillment of the requirements for the degree of

Master of Science
in
Mechanical Engineering

Alexander Leonessa, Chair
Alan Asbeck
Sunwook Kim

April 28, 2023
Blacksburg, Virginia

Keywords: biomechanical modeling, shoulder exoskeleton, design optimization

Biomechanics-Based Optimization for Exoskeleton Design

Melanie L. Hook

(ABSTRACT)

The goal of this thesis is to use biomechanical data describing shoulder motion to determine optimal parameters to assist in the design of a 5 DOF active shoulder exoskeleton. This thesis will provide a proof of concept on optimization techniques using motion data using a simplified 3 DOF model to facilitate future work implementing a full 5 DOF model. Optimization will be performed to determine the link lengths and, consequently, the locations of the joints of the exoskeleton by considering the human's workspace to maximize range of motion and promote user safety by minimizing collisions of the exoskeleton with the user and with the exoskeleton itself. The thesis will detail the development of computational models of the human and proposed exoskeleton, the processing of experimental data used to estimate the human's capabilities, optimization, and future work. This work will contribute to a large-scale NSF-funded project of building an upper body exoskeleton emulator. The emulator will promote the widespread adoption of exoskeletons in industry by providing a test-bed to streamline the rapid design of various assistance profiles for various users and tasks.

Biomechanics-Based Optimization for Exoskeleton Design

Melanie L. Hook

(GENERAL AUDIENCE ABSTRACT)

An exoskeleton is a robotic assistive device used in industrial and rehabilitative settings. This thesis will use data describing how the human shoulder moves during certain tasks to help design an exoskeleton to assist with theses tasks. A model of the human shoulder and a model of the exoskeleton will be developed and used in an optimization to figure out the best dimensions of the exoskeleton links to support the human's movements.

Acknowledgments

I would like to thank Dr. Leonessa and the members of my committee, Dr. Asbeck and Dr. Kim. I would also like to thank the NSF Graduate Research Fellowship Program for funding me. I could have not completed this degree without the many friends, TREC lab colleagues, and others I have met during my time at Virginia Tech who have supported me both academically and emotionally throughout this journey, especially Suyeon, Isaac, Carlo, Jyotshna, Bhaben, Ivan, and Mary. I am grateful for the support of my family (especially Mom, Dad, Michael, Dana, Josie, Gram, and Pap), friends, bandmates, my dog, and everyone who believed in me. Finally, music has been a huge form of emotional support so I would also like to acknowledge Motionless in White for always being there for me.

Contents

List of Figures

List of Tables

List of Algorithms

List of Abbreviations

AC Acromioclavicular Joint

ADL Activities of Daily Living

DH Denavit–Hartenberg

DOF Degrees of Freedom

DSEM Delft Shoulder and Elbow Model [2]

GH Glenohumeral Joint

ISB International Society of Biomechanics

MEDARM Motorized Exoskeleton Device for Advanced Rehabilitation of Motor Function [4, 5]

ROM Range of Motion

SC Sternoclavicular Joint

SHM Scapulohumeral Rhythm

ST Scapulothoracic Joint

Chapter 1

Introduction

The goal of this thesis is to use biomechanical modeling and data to optimize parameters for an upper body exoskeleton, focusing on the shoulder joint. Therefore, this chapter begins by explaining the importance of understanding the anatomy of the shoulder as it relates to movement capabilities. This chapter also provides the context behind the development of this exoskeleton by introducing existing exoskeletons, their applications and common design considerations, and barriers to widespread use of the technology. Some existing literature focusing on the development and use of shoulder models for exoskeleton design similar to the scope of this thesis and those are also summarized in this chapter. This introduction chapter will conclude by outlining the goals of the subsequent chapters.

1.1 Shoulder Anatomy

Figure 1.1 shows the main bones making up the shoulder complex including the scapula, humerus, clavicle, and sternum. Shoulder movement occurs as a result of contributions from four main joints connecting these bones: the glenohumeral (GH) joint, the acromioclavicular (AC) joint, sternoclavicular (SC) joint, and scapulothoracic (ST) joint. The ST joint is classified as a functional joint, rather than a true anatomical joint and therefore is generally not considered when modeling the shoulder. However, this joint is worth mentioning as the translation of the scapula, often referred to as scapulohumeral rhythm (SHM), is responsible

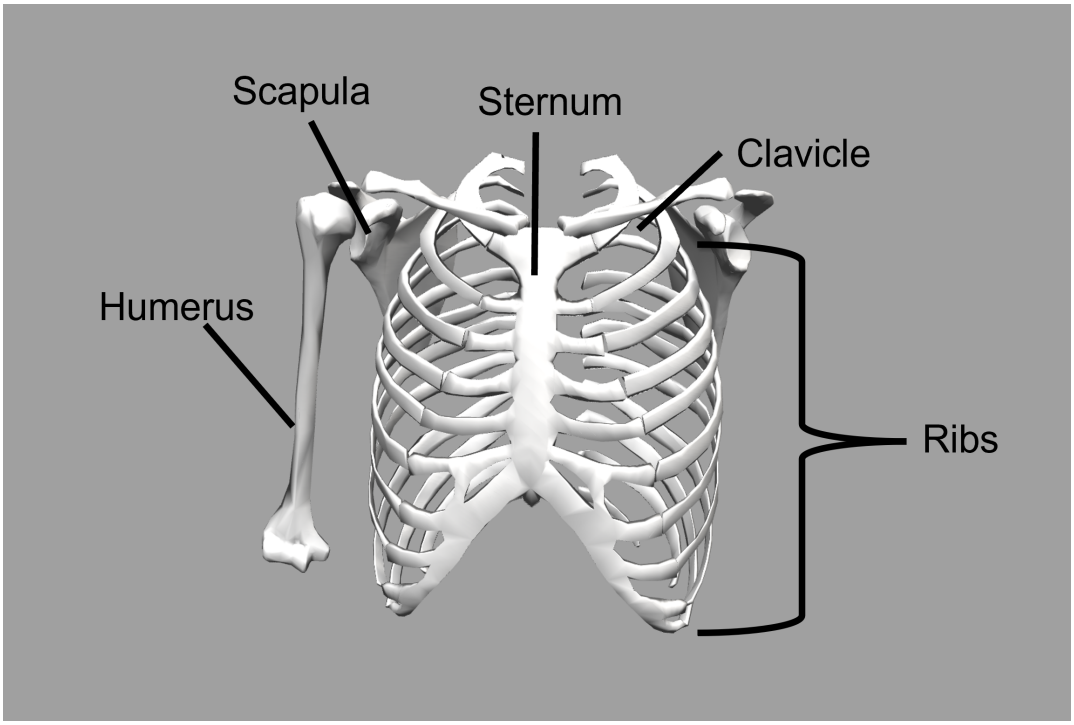

Figure 1.1: Bones of the Shoulder Girdle

for the translation of the GH joint to produce movements such as elevation/depression and protraction/retraction [6]. The SC joint between the sternum and clavicle connects the axial skeleton to the appendicular skeletona and is the main joint responsible for SHM. The AC joint connects the acromion of the scapula and the lateral end of the clavicle, but, due to the lack of direct muscle attachments, the movements of the AC joint are passive, resulting from the movement of surrounding joints. Finally, the GH joint acts similarly to a spherical ball-and-socket joint and is the articulation of the head of the humerus and the glenoid fossa of the scapula. The GH is the main joint involved in the 3 rotational degrees of freedom (DOF) of the shoulder.

The five main anatomical motions of the shoulder include flexion/extension, abduction/adduction, medial/lateral rotation, scapular protraction/retraction, and scapular elevation/depression, as shown in Figure 1.2 from [1]. These motions can be described using

the three standard anatomical planes of motion, also shown in Figure 1.2: the frontal (blue), sagittal (red), and transverse (green) planes. The frontal plane is an imaginary bisector splitting the body into front and back halves. GH abduction/adduction and scapular elevation/depression occur within this plane. The sagittal plane splits the body into left and right halves and the shoulder motion of flexion/extension occurs in this plane. Finally, the transverse plane, which bisects the body into upper and lower halves, is the plane of motion for medial and lateral rotation of the shoulder. Scapular protraction/retraction, another translational DOF of the shoulder, does not occur in only one anatomical plane, but rather the plane following the contour of the rib cage. However, [1] and other models simplify this motion to the sagittal plane, as shown in Figure 1.2. Many functional movements, such as those required during activities of daily living (ADL) or during repetitive occupational tasks, are multiplanar, resulting from various combinations of the five main anatomical motions.

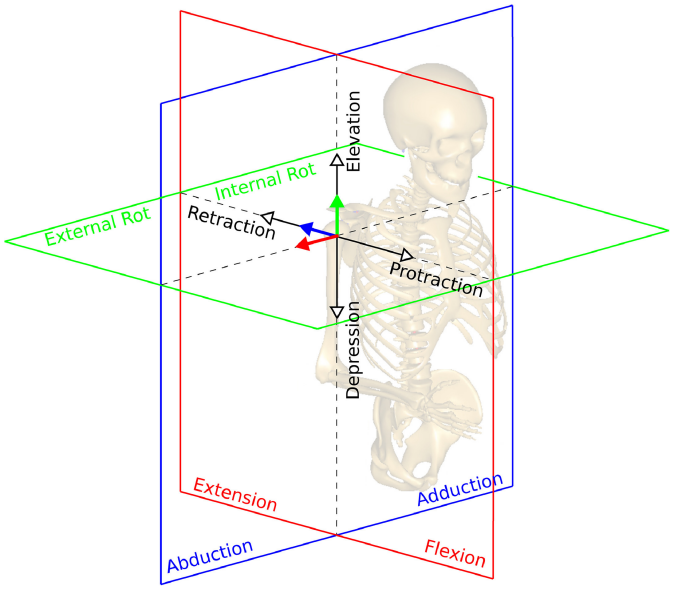

Figure 1.2: Anatomical Planes and Motions of the Shoulder [1]: Rotations occur about the colored axes perpendicular to the corresponding planes and translations occur along the black arrows.

Table 1.1 shows the average range of motion (ROM) of shoulder flexion/extension,

abduction/adduction, and medial/lateral rotation with respect to anatomical position as determined by [3].

Table 1.1: Shoulder Rotation Ranges of Motion [3]

Movement	Mean	SD	5th	95th
Shoulder Flexion	188	12	168	208
Shoulder Extension	61	14	38	84
Shoulder Abduction	134	17	106	162
Shoulder Adduction	48	9	33	63
Shoulder Medial Rotation	97	22	61	133
Shoulder Lateral Rotation	34	13	13	55

1.2 Existing Exoskeletons

1.2.1 Overview: Rehabilitative vs Industrial Exoskeletons

The majority of exoskeletons in the literature can be classified into two major categories based on their intended application: rehabilitation and industrial.

The goal of rehabilitation exoskeletons and robotics is to help patients with compromised motor function, such as those suffering from stroke, spinal cord injuries, sports injuries, etc., to regain the ability to perform activities of daily living. Robots provide several functions within the scope of rehabilitation, ranging from providing assistance, augmenting human power, and providing manual therapeutic operation in place of a physical therapist. Exoskeletons are beneficial in that they are more effective and less time-consuming than traditional physical therapy methods [7].

Exoskeletons in industry, on the other hand, are used primarily to enhance workers'

physical capabilities, therefore reducing the prevalence of work-related musculoskeletal disorders. Many industry-related injuries occur due to overexertion of the low back, shoulders, and arms, but exoskeletons can be easily implemented due to their portability and mobility to increase worker safety and productivity and reduce the user's physical demands [8].

1.2.2 Design Considerations

There are many design considerations that are common to both rehabilitative and industrial settings. For example, exoskeletons can provide unilateral assistance or bilateral assistance, but one drawback of bilateral designs is the increased potential of self-collision of the robot. Another consideration, heavily dependent on the overall intended use of the robot is the actuation. Designers need to consider which joints to actuate (single segment or multi-segment), the number of degrees of freedom to actuate for each segment, whether the DOFs should be passive or active, and finally the actuation method (electric, hydraulic, pneumatic, etc.). The exoskeleton's range of motion is also important to consider, with rehabilitative focusing more on matching the requirements of ADL and overall human range of motion, while industrial is generally more task-specific [7]. Safety of the user is also a priority; the exoskeleton should mimic natural human motion, avoid overextension of joints, and be customizable to individual anthropometry to increase comfort and reduce set-up time. Technical design objectives commonly include the avoidance of singularities in the desired workspace and collisions between the human and the exoskeleton and the exoskeleton and itself [4, 5]. Other design requirements include a high power-to-weight ratio, low complexity, low manufacturing cost, modularity access, low home usage cost, and high accuracy [7].

Rehabilitative exoskeletons are different than industrial ones in that they must provide therapeutic functionality, the requirements of which change based on the patient's current

condition. The exoskeleton is expected to accommodate the range of motion of functional reaching movements and a large range of assistance levels/training modes ranging from, such as active, passive, assistive, and resistive. Gravity compensation and simulating virtual environments such as moving through a viscous fluid or adding the weight of an object being picked up, are also commonly incorporated in rehabilitation settings [4, 5].

1.2.3 Barriers to Widespread Adoption

Industrial exoskeletons are generally evaluated subjectively via qualification of comfortability, usability, acceptance, injury risk, and/or perceived workload, or objectively via quantifications of muscular demands, kinematics, and/or metabolic cost [8]. However, since there is a lack of standardized testing methods and procedures, results from various studies are conflicting and there often exists discrepancies between lab and field results. Consequently, debate about the level of benefit from implementing exoskeletons is one barrier preventing a more widespread implementation in industry [8]. The authors in [9] acknowledge some of the other major deterrence for adoption of exoskeletons as optimization parameters for their exoskeleton: misalignment and interference between human and exoskeleton, and overall bulkiness. High interaction forces between the human and exoskeleton produced by a misalignment of exoskeleton and human joints results in discomfort for the user and is an especially prevalent problem for passive exoskeletons. The location of the joint mechanisms is also a common problem; since joints are commonly located above the shoulder, there is an increased risk of collision of the robot with the human's head and additional limitations of range of motion during overhead tasks. Finally, many current industrial exoskeletons simplify their design to focus on actuation of one DOF to reduce the overall weight and bulk, but this solution often amplifies misalignment and interference issues.

Rehabilitation exoskeletons face similar barriers to adoption as industrial, especially the lack of evaluation and safety concerns. Currently there is not enough testing in clinical settings to support device feasibility compared to traditional therapy methods. Additionally, advancement needs to be made to improve functionality parameters such as range of motion, modularity, and reconfigurability. Like industrial exoskeletons, the high interaction forces associated with poorly aligned rehabilitation exoskeletons present another concern. A final deterrent was the cost to implement the technology in clinical settings [7]. Many of the current exoskeletons mentioned in the next section address these issues by developing models of the shoulder to assist in the design of the exoskeleton with the user's anatomy in mind.

1.2.4 Shoulder Models

This section describes the methods used by several existing upper body exoskeletons to model the human's shoulder joint and conduct biomechanically-based design optimization.

There are many existing upper body exoskeletons that ignore the motion of the shoulder girdle to only actuate three DOFs to mimic the movements of the GH joint. These exoskeletons are generally not attached to the upper arm to reduce the risk of kinematic incompatibility and allow for simpler designs [6]. Others partially accommodate motion of shoulder girdle. Some add one additional DOF while others incorporate both degrees of freedom of the shoulder joint using partially or fully passive actuation methods. These types of exoskeletons generally take advantage of self-aligning mechanisms but lose the capability to actively actuate all degrees of freedom [6]. This thesis chooses to focus on the existing exoskeletons that actively actuate five or more degrees of freedom.

MEDARM [4, 5]

The Motorized Exoskelton Device for Advanced Rehabilitation of Motor function (MEDARM) is a rehabilitation exoskeleton with five actively actuated DOFs at the shoulder. The intersection of the three axes of rotation align with the user's GH joint. The authors of the paper chose to define one of the three axes to be parallel with the axis of revolution of the elbow joint at a resting configuration (anatomical pose) and optimized for the orientations of the other two axes based on the goals of matching the human's workspace, avoiding singularities, maximizing manipulability, and avoiding collisions with the human and the exoskeleton itself. The other two DOFs representing translation of the shoulder girdle was accomplished via a curved track system offset from the human with axes aligning with the user's SC joint, defined to be in the forward/horizontal direction for elevation/depression and the vertical/upward direction for protraction/retraction.

Harmony [6]

Similar to MEDARM[4, 5], the Harmony exoskeleton also uses a spherical joint to represent GH rotations with axes intersecting at the user's GH joint and one axis defined perpendicular to the sagittal plane (same as MEDARM) while the other two are optimized. Their optimization considerations included the shape and volume of actuators and the tradeoff between large range of motion and likelihood of singularities. Their optimization process was conducted using trial and error via 3D-printed mockups, as they argued that, "the interactions between the complex surfaces of the human body, actuator units, and linkages are impossible to model accurately." To accommodate the translation of the GH joint, Harmony chose to characterize the scapulohumeral rhythm via motion capture data collection, rather than use the SC joint as a user-exoskeleton alignment parameter like MEDARM.

They determined via motion capture that the GH joint follows circular arcs centered at a point not aligning with the SC joint, varying by subject body size, flexibility, etc. Their system was adjustable with respect to this pivot point and relevant link lengths. They focused on protraction/retraction and elevation/depression due to their contribution to SHM, but chose to ignore the third DOF at the SC joint (anterior-posterior axial rotation), citing that this DOF increases GH joint ROM but does not add an additional degree of freedom. They accounted for elevation/depression using a revolute joint with axis aligning with the center of the GH trajectory arc. They considered various placements for a revolute joint for protraction/retraction, but eliminated these configurations based on the collision risk of a bimanual design, reduction of arm ROM near the torso, and kinematic discrepancies, choosing to use a parallelogram mechanism instead.

Schiele [10]

Schiele used Dehavit-Hartenberg (DH) notation and the standard coordinate systems defined by the International Society of Biomechanics (ISB) [11] to create a 5 DOFs shoulder model, focusing on generating a motionspace similar to that of a human, rather than prioritizing precise modeling of biological components. They treated the GH joint as a 3 DOFs spherical joint and only considered sternoclavicular protraction/retraction and elevation/depression, omitting axial rotation, citing that it had "little effect on the positioning of the humerus bone." They also ignored the scapulothoracic and acromioclavicular joints because these biological joints are not required to describe "external" upper arm motion. The contributions of these joints, however, were incorporated into their artificially generated movement trajectories for 5th-95th percentile males corresponding to shoulder circumduction, abduction, horizontal retro-anteversion of 90 degree abducted arm, shoulder elevation/depression and protraction/retraction. Their goals were to avoid singularities, determine the best position

of human/exoskeleton attachment sites, and avoid collisions by maximizing the minimum distance between the exo's limbs and the human envelope. They found that a 6 DOFs exoskeleton exceeding the human's 5 DOFs was preferred to avoid collisions during complex motions such as circumduction. Their design consisted of a spherical joint (three revolute DOFs) with orthogonal axes intersecting at a point on the longitudinal humeral axis and a planar mechanism (two revolute DOFs + one prismatic DOF) to position the spherical joint. By using this planar mechanism instead of aligning the exoskeleton to human joints, which is difficult to do because of the muscles, tissues, and skin covering the precise location, their exoskeleton has reduced adjustment time, a greater workspace, and no risk of altered human/exoskeleton interaction due to misalignment or slippage.

1.3 Purpose of This Thesis

The work in this thesis will contribute to a larger National Science Foundation (NSF)-funded project to create an upper body exoskeleton emulator. The goal of this emulator is to promote the widespread adoption of exoskeletons in industry by providing a test-bed to streamline the rapid design of various assistance profiles for various users and tasks. This system will enable quicker prototyping of new ideas and help to decrease the time and cost of the overall design process. As this intended use is very broad, it is important that the exoskeleton is capable of matching the human's capabilities in terms of both range of motion and actuation to maximize the possible assistance profile options. This project will help fill the gap in the literature: currently, there is no industrial exoskeleton in the literature that is able to provide active assistance of all five DOFs of the shoulder. Therefore, properties of both industrial (augmentative torque requirements, etc.) and rehabilitative exoskeletons (range of motion, number of DOFs actuated, etc.) will need to be incorporated into the

overall design.

The goal of this thesis is to determine parameters to assist in the design of a 5 DOFs active shoulder exoskeleton. This thesis will provide a proof of concept on optimization techniques using biomechanical data using a simplified 3 DOFs exoskeleton model to facilitate future work implementing the full 5 DOFs. Optimization will be performed to determine the link lengths and, consequently, the locations of the joints of the exoskeleton by considering the human's workspace to maximize range of motion during various tasks quantified using experimental motion capture.

Chapter 2 will detail the development of computational models of the human and proposed exoskeleton. Chapter 3 will discuss the experimental data used to estimate the human's capabilities. Chapter 4 will describe the optimization objectives and algorithms. Finally, Chapter 5 will discuss the results and conclusions, along with future optimization work incorporating more robust human and exoskeleton models.

Chapter 2

Modeling

This chapter describes the development and use of two separate models: the human shoulder and the initial design of the exoskeleton. For the human model, the required degrees of freedom and relevant assumptions are explained, along with the coordinate systems used to describe joint movements and anthropometric information about the subject used. This information is all compiled into a 3 DOFs Simulink model and a full 5 DOFs model. This chapter also explains the proposed structure of a 3 DOFs exoskeleton, which can be modified to 5 DOFs in future work. The exoskeleton is modeled similarly in Simulink. Additionally, a computational DH model is developed and used for forward and inverse kinematic simulations.

2.1 Human Model

2.1.1 Degrees of Freedom

As mentioned in the introduction, the acromioclavicular joint movement is passive, resulting from movements of surrounding joints. Therefore, it has been decided follow the standard practice of other models in the literature to ignore contributions of this joint. Similarly, the scapulothoracic joint, a functional joint rather than true anatomical joint, will also be omitted from the model presented in this thesis. The two joints to be considered are the

glenohumeral joint (3 DOFs) and the sternoclavicular joint (3 DOFs). However, only the two DOFs of the SC joint responsible for elevation/depression and protraction/retraction will be considered. The third DOF, anterior-posterior axial rotation, can be omitted following the logic of [6], where the authors argued that this DOF increases GH joint ROM but does not add an additional degree of freedom.

One assumption associated with the simplification of the shoulder joint to the five DOFs mentioned is that the joint's arthrokinematics are negligible and the corresponding movement can be represented using pure revolute joints. Joint biomechanics can be described through both osteokinematics, the externally visible limb movement, and arthrokinematics, the externally invisible rolling, spinning, and sliding movements between joint surfaces. The majority of existing shoulder models simplify joints to only consider their osteokinematics. For example, the GH joint is commonly modeled as a 3 DOFs ball-and-socket (spherical) joint based on the osteokinematic functions of flexion/extension, abduction/adduction, and medial/lateral rotation. However, when considering joint arthrokinematics, the GH joint is not a true spherical joint; flexion/extension are caused by spin, adduction/abduction are caused by superior and inferior gliding respectively, and medial/lateral rotations are caused by posterior and anterior glide respectively. The assumption made in many models including the one presented in this thesis is that the joints of the shoulder can reasonably be simplified to neglect arthrokinematics such that the GH joint can be considered three coincident revolute joints and the SC joint two coincident revolute joints.

While it is evident that a full 5 DOFs shoulder model is necessary for the exoskeleton emulator application, this thesis presents a proof-of-concept for the optimization algorithm, studying a 3 DOFs exoskeleton to accommodate GH motion only. This thesis assumes that these three degrees of freedom can be optimized separately from the two translational DOFs of the shoulder girdle if the future mechanism for the additional DOF is able to sufficiently

track the translational movement of the GH joint so that distal joints of the exoskeleton align with the human's anatomical joint.

2.1.2 Coordinate Systems/Anthropometry

The ISB created a recommended upper limb joint coordinate system convention [11]. Figure 2.1 shows the local coordinate systems and rotations of the SC and GH joints. The SC joint follows a YXZ Euler angle rotation sequence and the angles match conventional anatomical naming. The two degrees of freedom considered in this thesis are SC pro/retraction (PR), which occurs due to rotation about the SCy axis and causes forward/backward translation of the GH joint, and SC elevation/depression (ED), which occurs due to rotation about the SCx axis and causes up/down translation of the GH joint. The ISB recommends a YXY Euler sequence to describe the rotations of the GH joint, but work done by [12] suggests that an XZY sequence is more effective, thus the XZY convention will be used in this thesis. The angles defined by this convention do not directly correspond to traditional anatomical motions mentioned in Ch. 1, so they will be referred to as GHx, GHy, and GHz based on their respective rotation axes.

The next step in the modeling process is to determine the relevant anthropometry. Ideally, this data would be personalized based on the individual, but initial iterations of the model utilized the anthropometric properties of the Delft Shoulder and Elbow Model (DSEM). The DSEM is a widely accepted and utilized upper limb model from which anthropometry, validated in [13], could be extracted: the relative location of relevant joints and landmarks, bone geometry, mass and inertial properties, etc. Table 2.1 lists the distance in meters from the SC joint to the GH joint with respect to the SC coordinate system and from the GH joint to the elbow joint with respect to the GH coordinate system for the DSEM

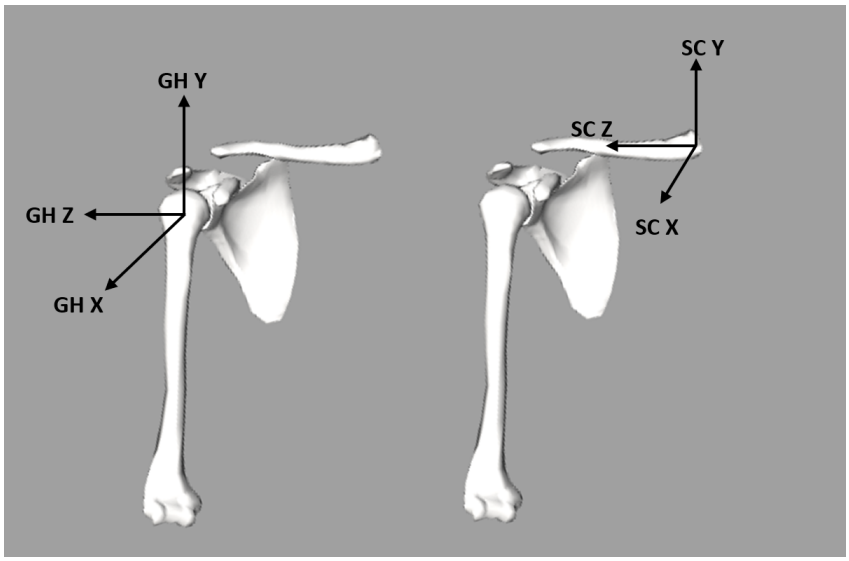

Figure 2.1: ISB coordinate systems and movements of the GH (left) and SC (joints)

subject used to construct the model.

Table 2.1: Anthropometric Distances

Distance	X (m)	Y (m)	Z (m)
GH wrt SC	0	-0.0317	0.182
Elbow wrt GH	0	-0.2907	0.005

2.1.3 Simulink Model

For a 3 DOFs model, the GH joint was modeled using three coincident revolute joints using massless intermediate links with zero lengths. Rigid body transform blocks were used to match the orientation and translation of the joint coordinate systems with respect to the previously described coordinate system conventions and the anthropometric data from the Delft model. Inputs to the model from the Matlab workspace include the GHx, GHy, and GHz Euler rotation angles. The output, required for forward kinematics/workspace analysis (Ch. 2.1.5), is the transformation matrix of the elbow with respect to the global frame.

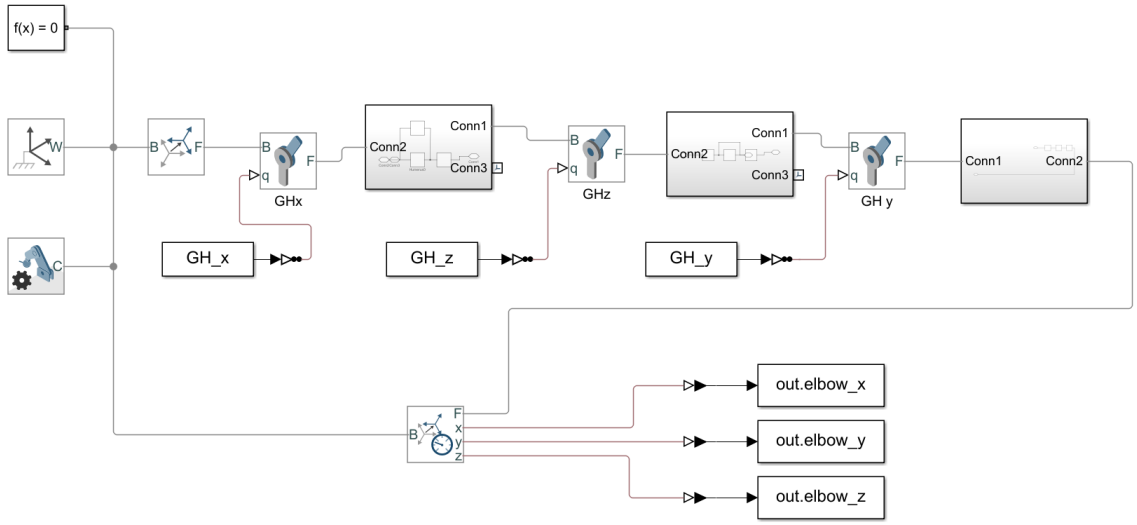

Figure 2.2: 3 DOFs Simulink Human Shoulder Model Block Diagram

Figure 2.2 shows the Simulink block diagram of the model.

The 3 DOFs model was expanded to include the additional two DOFs of the SC using similar modeling methods and the anthropometric distances listed in Table 2.1, and the resulting Simulink block diagram is shown in Figure 2.3. For visualization purposes, the scapula bone was added to the model using a weld joint for the AC joint, as its movements were omitted as previously explained.

Performing forward kinematics to output the end effector configuration using the Simulink model is straightforward through the use of a TransformSensor block connecting the desired frames, in this case, the global frame and the coordinate frame located at the elbow. For the 3 DOFs model, the global frame was located at the GH joint so the resulting trajectory of the elbow is only reflective of GH movement. The global frame of the 5 DOFs model was located at the SC joint so the resulting trajectory of the elbow incorporates the translation of the GH joint due to SC movement.

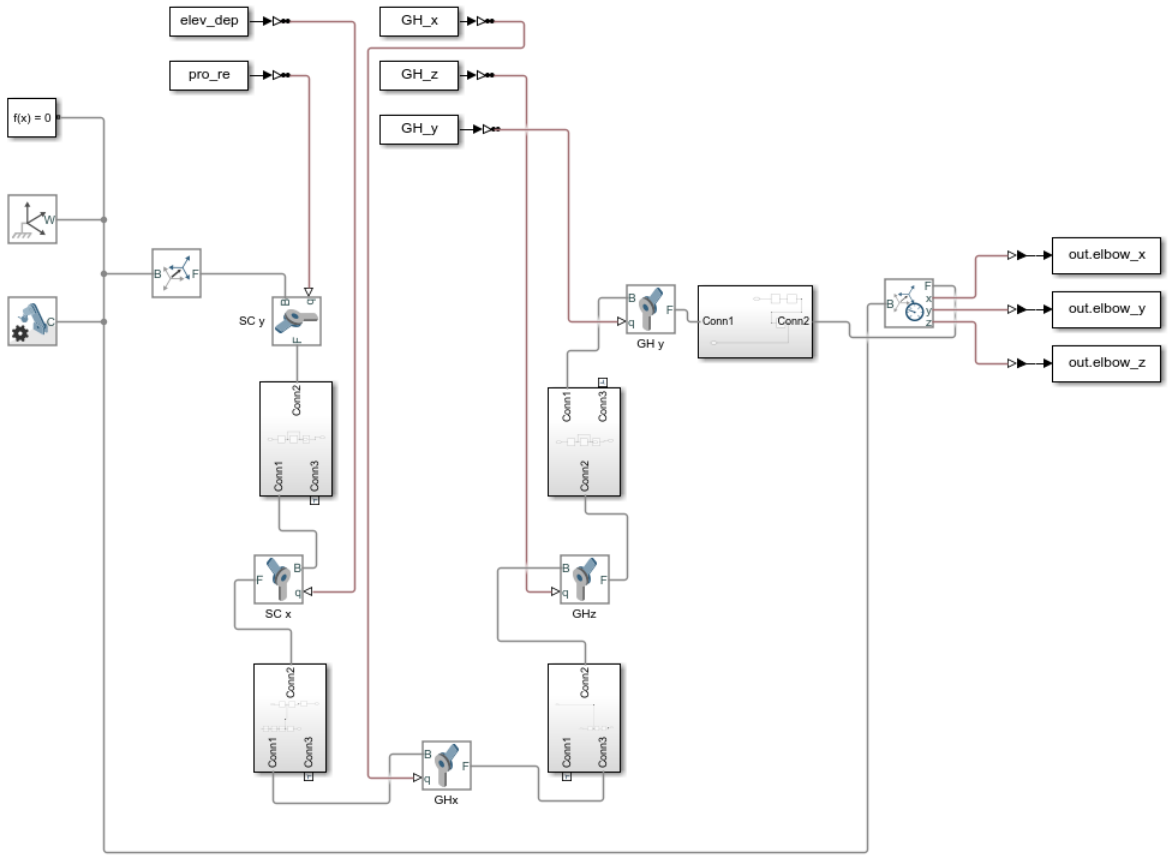

Figure 2.3: 5 DOFs Simulink Human Shoulder Model Block Diagram

2.2 Exoskeleton Model

The majority of existing exoskeletons in the literature agree on a standard accommodation of the motions of the GH joint using three revolute joints whose axes intersect at the human's GH joint. Therefore, it was decided that the optimization of these three DOFs could be performed as a subset of the overall design process, assuming that the other two DOFs would not interfere with the distal links and would be able to track the GH joint for sufficient alignment of distal joints. The first exoskeleton model presented in Ch. 2.2.1 contains only the bodies relevant to the GH DOFs. Future work will address addition and optimization of

parameters related to the extra DOF of the shoulder girdle.

2.2.1 Simulink Model

To account for the spherical GH joint, three rotational degrees of freedom are required. Following the standard practice in exoskeleton design in the literature, the three axes of rotation of the exoskeleton's revolute joints will be configured such that their intersection aligns with the human's GH joint location, however the angles between these axes are unknown, to be determined during the optimization phase in later sections.

The initial design for this portion of the exoskeleton consists of three rectangular bodies, shown from a transverse plane view in Figure 2.4. The thickness of these bodies was chosen arbitrarily. The blue and green bodies are intended to be curved, but will be approximated as two straight sub-links connected by a weld joint for modeling simplicity. The angles and lengths required for Simulink rigid body transformations connecting the sub-links were computed using geometric and trigonometric relationships.

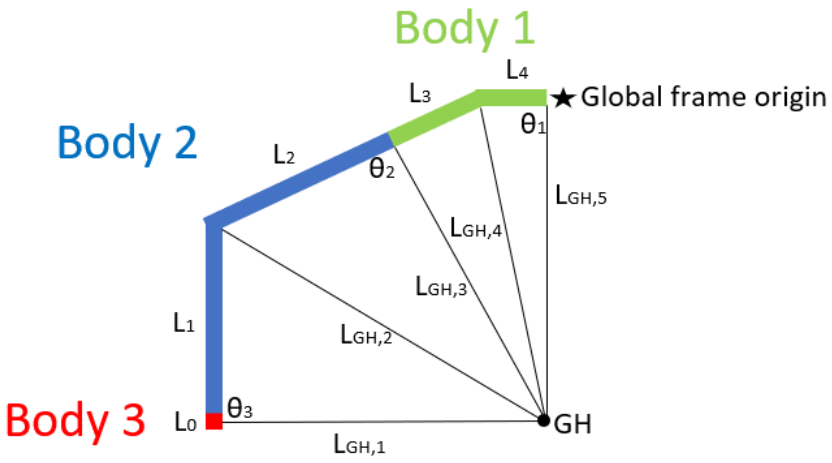

Figure 2.4: Top view of Simulink model exoskeleton bodies with arbitrary link lengths

In the model, the main bodies are joined by three revolute joints: θ_1 between Body 1 (green) and the global frame, θ_2 between Body 1 and Body 2 (blue), and θ_3 between Body 2 and Body 3 (red). When worn by the user, the red Body 3 (extending into the plane of the page with a length of L_5) would attach rigidly to the human's upper arm. The model design inputs for optimization include the distance from θ_1 to the human user's GH joint ($L_{\mathrm{GH},5}$) and the link lengths L_0 L_1, L_2, L_3, and L_4. The other L_{GH} distances are derived parameters dependent upon optimized parameters and will be relevant when defining optimization constraints in future chapters.

Similar to the construction of the human model, the Simulink block diagram consists of revolute joints, rigid bodies, rigid body transforms, as shown in Figure 2.5.

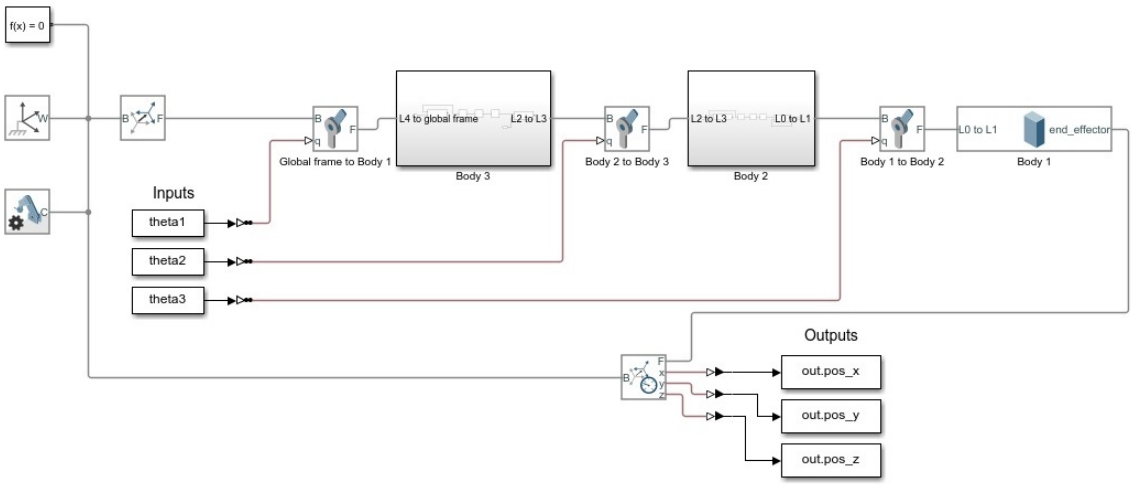

Figure 2.5: 3 DOFs Simulink Exoskeleton Model Block Diagram

2.2.2 Computational Model - DH Representation

Due to the added geometric complexity of the proposed design, the DH representation provided a systematic method for computing the transformation matrices. The coordinate systems for each link were chosen such that each z-axis aligned with the direction of the human joint axis. The x-axis was chosen to be perpendicular to the z-axis of the current frame and the z-axis of the previous frame. Finally, the y-axis was chosen to follow the right-hand rule. The origin of the coordinate frame was chosen such that the x-axis intersects with the z-axis of the previous frame. The coordinate system convention including the location and orientation of all relevant frames is shown in Figure 2.6.

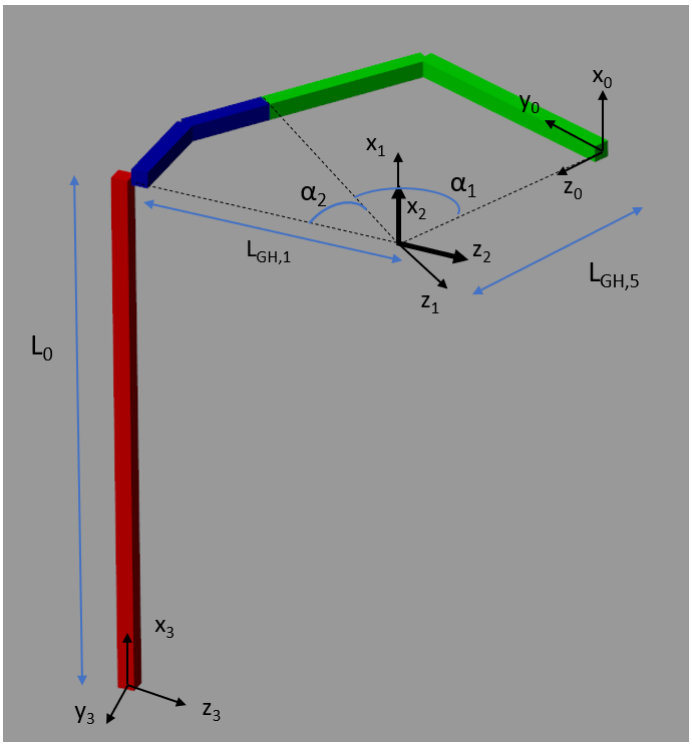

Figure 2.6: Exoskeleton DH Coordinate Systems

Consistent with the notation described in [14], N represents the frame number. Since all of the joints are revolute, the θ parameter, representing the rotation about Z_{n-1} required for X_{n-1} to match X_n, is the joint variable corresponding to the respective exoskeleton DOF.

α is the rotation about X_n required to get Z_{n-1} to match Z_n. D is the distance from the center of the $n-1$ frame to the center of the nth frame along the X_n direction. R is the distance from the center of the $n-1$ frame to the center of the nth frame along the Z_{n-1} direction. Table 2.2 shows the DH parameters with θ^* indicating joint variables.

Table 2.2: DH Parameters -Exoskeleton

n	θ	α	D	R
1	θ_1^*	α_1	$L_{\mathrm{GH},5}$	0
2	θ_2^*	α_2	0	0
3	θ_3^*	π	$-L_{\mathrm{GH},1}$	$-L_0$

L_0 and $L_{\mathrm{GH},5}$ are optimized parameters, while $L_{\mathrm{GH},3}$, α_1, and α_2 are derived quantities dependent on the optimized link lengths. The geometric and trigonometric equations for these variables can be found in the appendix.

Forward Kinematics

The end effector position can be computed forward kinematics using the standard methods incorporating the data found in the DH table (Table 2.2). The resulting transformation matrices are

$$T_{01} = \begin{bmatrix} \cos(\theta_1^*) & -\sin(\theta_1^*)\cos(\alpha_1) & \sin(\theta_1^*)\sin(\alpha_1) & 0 \\ \sin(\theta_1^*) & \cos(\theta_1^*)\cos(\alpha_1) & -\cos(\theta_1^*)\sin(\alpha_1) & 0 \\ 0 & \sin(\alpha_1) & \cos(\alpha_1) & L_{\mathrm{GH},5} \\ 0 & 0 & 0 & 1 \end{bmatrix}, \tag{2.1}$$

$$T_{12} = \begin{bmatrix} \cos(\theta_2^*) & -\sin(\theta_2^*)\cos(\alpha_2) & \sin(\theta_2^*)\sin(\alpha_2) & 0 \\ \sin(\theta_2^*) & \cos(\theta_2^*)\cos(\alpha_2) & -\cos(\theta_2^*)\sin(\alpha_2) & 0 \\ 0 & \sin(\alpha_2) & \cos(\alpha_2) & 0 \\ 0 & 0 & 0 & 1 \end{bmatrix}, \tag{2.2}$$

$$T_{23} = \begin{bmatrix} \cos(\theta_3^*) & -\sin(\theta_3^*)\cos(\pi) & \sin(\theta_3^*)\sin(\pi) & -L_0\cos(\theta_3^*) \\ \sin(\theta_3^*) & \cos(\theta_3^*)\cos(\pi) & -\cos(\theta_3^*)\sin(\pi) & -L_0\sin(\theta_3^*) \\ 0 & \sin(\pi) & \cos(\pi) & -L_{\mathrm{GH},1} \\ 0 & 0 & 0 & 1 \end{bmatrix}. \tag{2.3}$$

The product of transformation matrices between individual frames yields the transformation matrix from the origin frame to end effector frame, shown by the equation,

$$T_{03} = T_{01}T_{12}T_{23}. \tag{2.4}$$

Inverse Kinematics

While forward kinematics is the computation of end effector configuration based on joint positions, inverse kinematics is the opposite; inverse kinematics determines possible joint positions that yield a desired end effector position. In the context of this thesis, inverse kinematics is important to ensure that the end effector of the exoskeleton, connected to the user's upper arm, is able to reach a similar workspace to that of the human's upper arm.

Matlab was used to calculate the numerical solution to the inverse kinematics problem by first computing the joint velocity via

$$\dot{Q} = J^{\dagger} \ (\dot{X}_{\text{des}}(+\alpha \ (X_{\text{des}} - \text{RobotPos})), \tag{2.5}$$

where $J^{\dagger}$ is the pseudoinverse of the Jacobian, X_{des} is the desired position of the end effector, α is the step size, $\dot{X}_{\text{des}}$ is the desired joint velocity, and RobotPos is the position of the robot for a given set of angles based on the transformation matrix derived previously in Eqn 2.4.

Using $\dot{Q}$ as the output of a function, like the one shown in Algorithm 1, Eqn 2.5 can then be integrated numerically using an ordinary differential equation solver, in this case Matlab's ode15s function. The InverseKinematics function requires the link lengths (x), symbolic representations of the exoskeleton joint angles (Q), and desired end effector position (elbow_position) as inputs. α is a heuristic step size, in this case chosen to be the identity matrix. The desired end effector position is based on human movement trajectories and discussed further in Ch. 3. The desired velocity was set to zero, since the goal was to determine whether or not individual desired positions were within the workspace, rather than follow a specific, velocity-dependent motion.

Algorithm 1 Inverse Kinematics

Solve InverseKinematics function using Matlab ODE solver with initial guess θ_0 and heuristic time range

$Q = ode45(\text{InverseKinematics}, 0 : timestep : t_{\text{final}}, \theta_0)$

function InverseKinematics(x, Q, elbow_position)

Set step size: $\alpha = \begin{bmatrix} 100 \\ 010 \\ 001 \end{bmatrix}$

Desired robot position: $X_{\text{des}} = \text{elbow\_position}$

Desired robot velocity: $\dot{X}_{\text{des}} = \begin{bmatrix} 0 \\ 0 \\ 0 \end{bmatrix}$

Compute Jacobian and its pseudo inverse, $J^{\dagger}$, as a function of x and Q

Compute end effector position: $T_{03} = T_{01}T_{12}T_{13}$
RobotPos $= T_{03}(1:3, 4)$

Compute $\dot{Q}$: $\dot{Q} = J^{\dagger}\ (\dot{X}_{\text{des}} + \alpha\ (X_{\text{des}} - \text{RobotPos}))$

Return $\dot{Q}$

end function

Chapter 3

Experimental Data

This chapter discusses the processing of open-source shoulder motion collected by Bosterlee et al. [2]. Using optical motion capture data, the coordinate frames for the clavicle and GH can be determined based on the recommended ISB conventions [11], which allows for the determination of the Euler angles of rotation responsible for the movement. The GH angle results are presented for full range of motion abduction, sagittal plane flexion, and scapular plane flexion for one subject studied by [2].

3.1 Motion Capture Data Collection

3.1.1 Marker Set

A subset of the open-source database of motion capture data describing various shoulder movements and ADL produced by [2] will be used in this thesis. They implemented the marker placement and naming conventions recommended by the ISB [11] and collected data using an Optotrak system and a frequency of 100 Hz. Only the markers used to determine the coordinate systems and joint angles relevant to this thesis are described in Table 3.1 and shown in Figure 3.1. All of these markers, with the exception of the GH joint center, can be placed on a subject using standard palpation procedures. The GH joint center cannot be externally located and therefore must be estimated numerically using a process such as the

instantaneous helical axis method described by [15].

Table 3.1: Marker Set

Abbreviation	Name	Description
AA	Angulus Acromialis	most lateral part of the back of the scapula
AC	Acromioclavicular joint	articulation between clavical and acromion of scapula
AI	Angulus Inferior	inferior angle of scapula
C7	7th cervical vertebrae	spinous process
EL	Epicondylus Lateralis	lateral epicondyle of the humerus
EM	Epicondylus Medialis	medial epicondyle of the humerus
GH*	Glenohumeral Joint	approximated location of rotational center of the GH joint
IJ	Incisura Jugularis	suprasternal notch of the sternum
PX	Xiphoid Process	most inferior part of the sternum
SC	Sternoclavicular joint	articulation between sternum and clavicle
TS	Trigonum spinae scapulae	root of the scapular spine
T8	8th thoracic vertebrae	spinous process

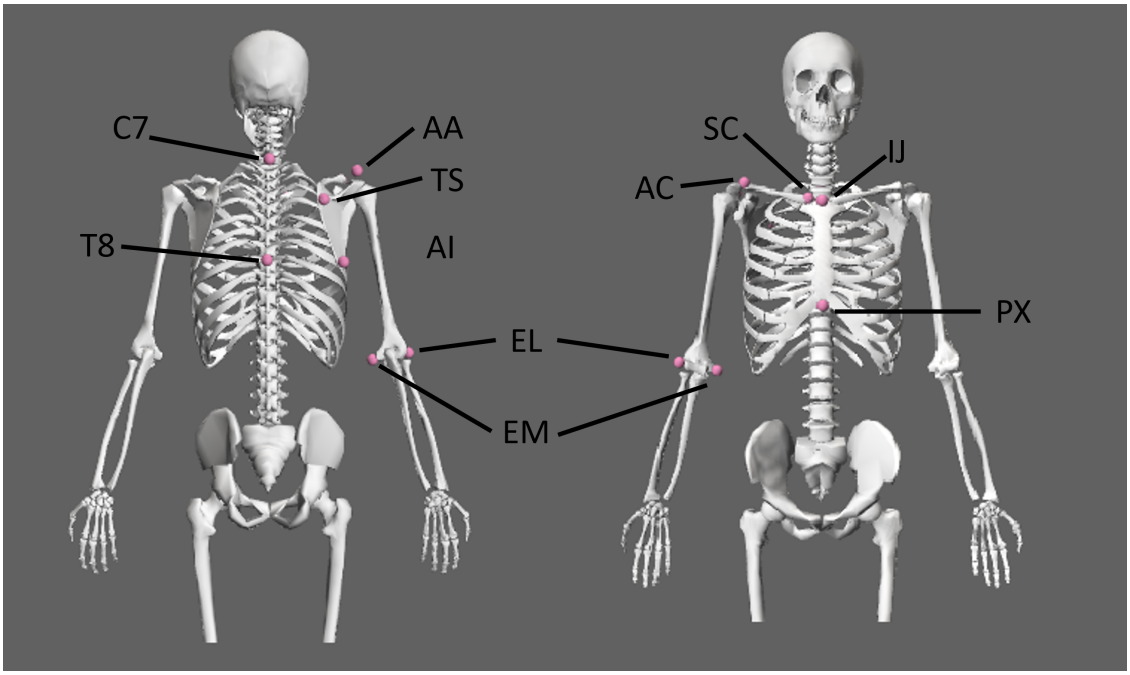

Figure 3.1: Markerset: Posterior (left) and anterior (right) views

3.2 Data Processing

Once marker data has been collected, the positions are used based on the ISB recommendations to compute the coordinate systems of each body from which the joint angles can be extracted over a trajectory. This was done by modifying code provided by [2].

3.2.1 Determination of Coordinate Frames

Clavicle Coordinate System

Acromioclavicular protraction/retraction and elevation/depression are computed with respect to the clavicle coordinate frame, the origin of which is located at the SC marker. The z axis of the clavicle frame was defined as the vector from SC to AC markers. The y axis was defined as the line perpendicular to the z axis and the upward-pointing axis between the midpoint of PX and T8 and the midpoint of IJ and C7. The y axis cross product of the x and z axes, pointing upward. For a given set of marker locations, the vector describing the orientations of these axes can be computed and organized as a rotation matrix where the first column is the orientation of the x axis, second column is the orientation of the y axis, and third column is the orientation of the z axis in that particular timestep. This procedure is summarized in the pseudocode of Algorithm 2.

GH Coordinate System

The three degrees of freedom of the glenohumeral joint occur about a coordinate system with origin located at the GH center of rotation. This location was estimated numerically using the process described by [15]. The y axis was defined to be the vector from the midpoint of the EL and EM markers to the GH. The x axis points in the forward direction, perpendicular

Algorithm 2 Computation of Clavicle Coordinate System Rotation Matrix

for $timestep = 1, 2, \ldots$ **do**

Compute z axis unit vector: $z = \frac{\text{AC}-\text{SC}}{||\text{AC}-\text{SC}||}$

Compute vector between midpoints: $\text{temp} = \frac{\text{IJ+C7}}{2} - \frac{\text{T8+PX}}{2}$

Compute x axis unit vector: $x = \frac{\text{temp}\times z}{||\text{temp}\times z||}$

Compute y axis unit vector: $y = z \times x$

Output rotation matrix: $R = [xyz]$

end for

to the frontal plane containing the GH, EL, and EM markers. The z axis is the cross product of the x and y axes pointing laterally. This procedure is summarized in the pseudocode of Algorithm 3.

Algorithm 3 Computation of GH Coordinate System Rotation Matrix

for $timestep = 1, 2, \ldots$ **do**

Compute y vector: $y = \text{GH} - \frac{\text{EM+EL}}{2}$

Unit vector: $y = \frac{y}{||y||}$

Compute x vector: $x = y \times \frac{\text{EM+EL}}{2}$

Unit vector: $x = \frac{x}{||x||}$

Compute z axis: $z = x \times y$

Output rotation matrix: $R = [xyz]$

end for

3.2.2 Computation of Euler Angles

Given the rotation matrices described previously, Euler angles can be extracted from the clavicle CS using a YXZ Euler angle order, per ISB recommendations, where relevant angles include rotations about the y axis (protraction/retraction) and x axis (elevation/depression). In order to obtain YXZ rotation angles from a rotation matrix, one factor the product of

three elementary rotation matrices $R_y(\theta_y)$, $R_x(\theta_x)$, and $R_z(\theta_z)$, each describing a rotation about a single standard axis. The elementary matrices are

$$R_x(\theta_x) = \begin{bmatrix} 1 & 0 & 0 \\ 0 & \cos(\theta_x) & -\sin(\theta_x) \\ 0 & \sin(\theta_x) & \cos(\theta_x) \end{bmatrix}, \tag{3.1}$$

$$R_y(\theta_y) = \begin{bmatrix} \cos(\theta_y) & 0 & \sin(\theta_y) \\ 0 & 1 & 0 \\ -\sin(\theta_y) & 0 & \cos(\theta_y) \end{bmatrix}, \tag{3.2}$$

$$R_z(\theta_z) = \begin{bmatrix} \cos(\theta_z) & -\sin(\theta_z) & 0 \\ \sin(\theta_z) & \cos(\theta_z) & 0 \\ 0 & 0 & 1 \end{bmatrix}. \tag{3.3}$$

Multiplying $R_y(\theta_y)$, $R_x(\theta_x)$, and $R_z(\theta_z)$ and simplifying, using c for cosine and s for sine, yields the following expression, which can be set equal to to the rotation matrix describing the orientation of the coordinate system

$$\begin{bmatrix} r_{11} & r_{12} & r_{13} \\ r_{21} & r_{22} & r_{23} \\ r_{31} & r_{32} & r_{33} \end{bmatrix} = \begin{bmatrix} c_y c_z + s_x s_y s_z & c_z s_x s_y - c_y s_z & c_x s_y \\ c_x s_z & c_x c_z & -s_x \\ -c_z s_y + c_y s_x s_z & c_y c_z s_x + s_y s_z & c_x c_y \end{bmatrix}. \tag{3.4}$$

Equating corresponding entries of the two matrices, the simplest solution for θ_x is $\text{asin}(-r_{23})$. Depending on the value of θ_x, there are different possible results for θ_y with each case outlined in Algorithm 4.

The ISB recommends a YXY Euler sequence [11], but work done by [12] suggests that

Algorithm 4 Computation of YXZ Euler angles

if -1 $< r_{23} <$ 1 **then**
$\theta_x = \text{asin}(-r_{23})$
$\theta_y = \text{atan2}(\frac{r_{13}}{r_{33}})$
$\theta_z = \text{atan2}(\frac{r_{21}}{r_{22}})$

else if $r_{23} = -1$ **then**
$\theta_x = \pi/2$
$\theta_y = -\text{atan2}(\frac{-r_{12}}{r_{11}})$
$\theta_z = 0$

else if $r_{23} = 1$ **then**
$\theta_x = -\pi/2$
$\theta_y = \text{atan2}(\frac{-r_{12}}{r_{11}})$
$\theta_z = 0$

end if

an XZY sequence is more effective for describing GH rotations. A similar procedure as described previously for the SC joint can be performed for the GH joint to extract angles from the rotation matrix, setting the rotation matrix equal to the the product of $R_x(\theta_x)$, $R_z(\theta_z)$, and $R_y(\theta_y)$ via the equation

$$\begin{bmatrix} r_{11} & r_{12} & r_{13} \\ r_{21} & r_{22} & r_{23} \\ r_{31} & r_{32} & r_{33} \end{bmatrix} = \begin{bmatrix} c_y c_z & -s_z & c_z s_y \\ s_x s_y + c_x c_y s_z & c_x c_z & -c_y s_x + c_y s_y s_z \\ -c_x s_y + c_y s_x s_z & c_z s_x & c_x c_y + s_x s_y s_z \end{bmatrix}. \tag{3.5}$$

Equating corresponding entries of the two matrices, the simplest solution for θ_z is $\text{asin}(-r_{12})$. Depending on the value of θ_z, there are different possible results for θ_x and θ_y described in Algorithm 5.

Algorithm 5 Computation of XZY Euler angles

if -1 $< r_{12} <$ 1 **then**
$\theta_z = \text{asin}(-r_{12})$
$\theta_x = \text{atan2}(\frac{r_{32}}{r_{22}})$
$\theta_y = \text{atan2}(\frac{r_{13}}{r_{11}})$

else if $r_{12} = -1$ **then**
$\theta_z = \pi/2$
$\theta_x = -\text{atan2}(\frac{-r_{31}}{r_{33}})$
$\theta_y = 0$

else if $r_{12} = 1$ **then**
$\theta_z = -\pi/2$
$\theta_x = \text{atan2}(\frac{-r_{31}}{r_{33}})$
$\theta_y = 0$

end if

3.3 Experimental Data Results

Initial testing was performed using sample data found in the literature collected by Bosterlee et al [2]. They investigated activities of daily living and full joint ranges of motion of the shoulder, specifically abduction, flexion in the sagittal plane, flexion in the scapular plane (45 degrees from the frontal plane) and endorotation. However, since our intended exoskeleton application is for industrial tasks, sagittal plane flexion, scapular plane flexion and abduction were the most relevant, but future motion capture work should expand to other movements.

3.3.1 Abduction

The subject from the [2] completed full range of motion abduction trials; the corresponding angle trajectories of the three relevant GH DOFs and two SC DOFs are shown in Figure 3.2 for both fast and slow speeds. During shoulder abduction, the arm moves in the frontal plane away from the midline of the body until the point of maximal humeral elevation. One

limitation of this data set from the literature is that the motion starts and ends with the arm hanging downward from the subject's side and does not consider the full adduction motion allowing the arm to cross the midline of the body. There is some angular motion of all degrees of freedom, but the motion is mostly caused by rotations about the X and Y axes of the GH joint.

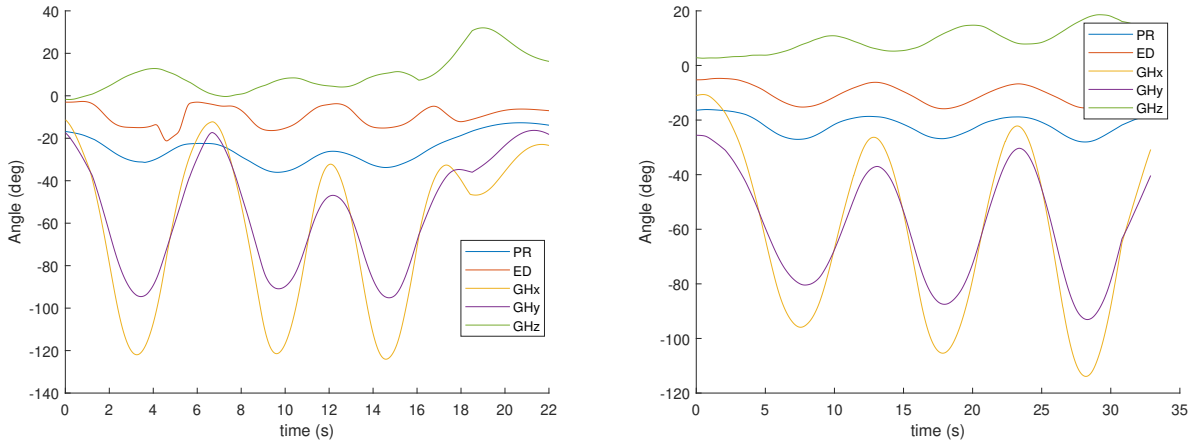

(a) Abduction - fast trial

(b) Abduction - slow trial

Figure 3.2: Full 5 DOFs angle trajectories for experimental abduction data collected by Bosterlee et al [2]

3.3.2 Sagittal Flexion

Similar to abduction, the subject begins with their arm hanging downward by their side and moves until reaching maximal humeral elevation, but this time in the sagittal plane. The subjected completed both fast and slow trials and the angle trajectories of all 5 DOFs are shown in Figure 3.3. A limitation of this dataset is that the movement is limited to full flexion and does not consider extension past the starting point. Compared to the slow trials, the subject achieves a slightly greater maximum angle for all 3 DOFs at the peak of the motion during the fast trials.

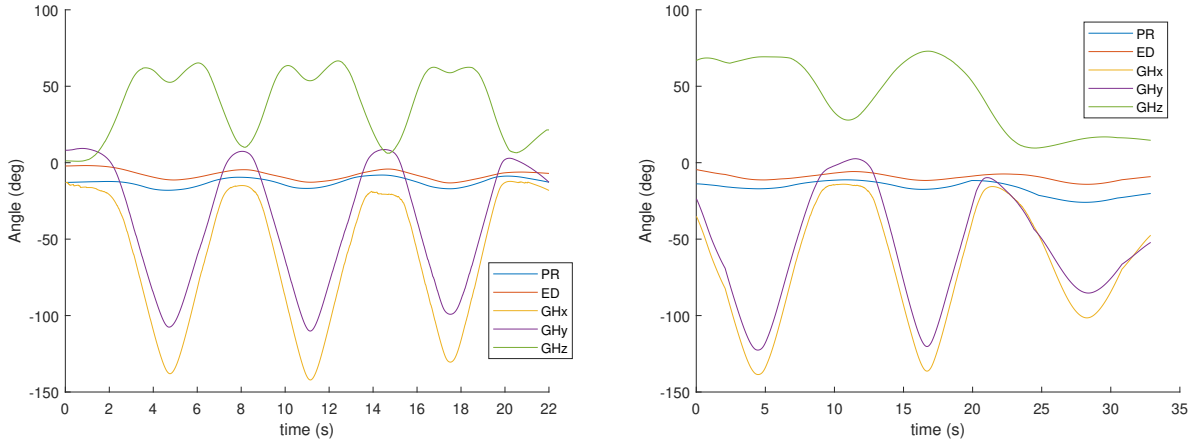

(a) Sagittal flexion - fast trial

(b) Sagittal flexion - slow trial

Figure 3.3: Full 5 DOFs angle trajectories for experimental sagittal flexion data collected by Bosterlee et al [2]

3.3.3 Scapular Flexion

Scapular flexion is similar to the previously described movements, but is performed in the scapular plane, 45 degrees from both the frontal and sagittal planes. The subjected completed both fast and slow trials and the angle trajectories of the 5 DOFs are shown in Figure 3.4. Compared to the fast trials, the slower tempo allows the subject to achieve a slightly greater maximum angle for all 3 GH DOFs at the peak of the motion, which is the opposite of the trend during sagittal flexion.

3.4 Forward Kinematics Results

The angle trajectories from the previous section were used in conjunction with the models developed in Ch. 2 to perform forward kinematics and estimate the position of the human's end effector (the elbow) during the trajectory.

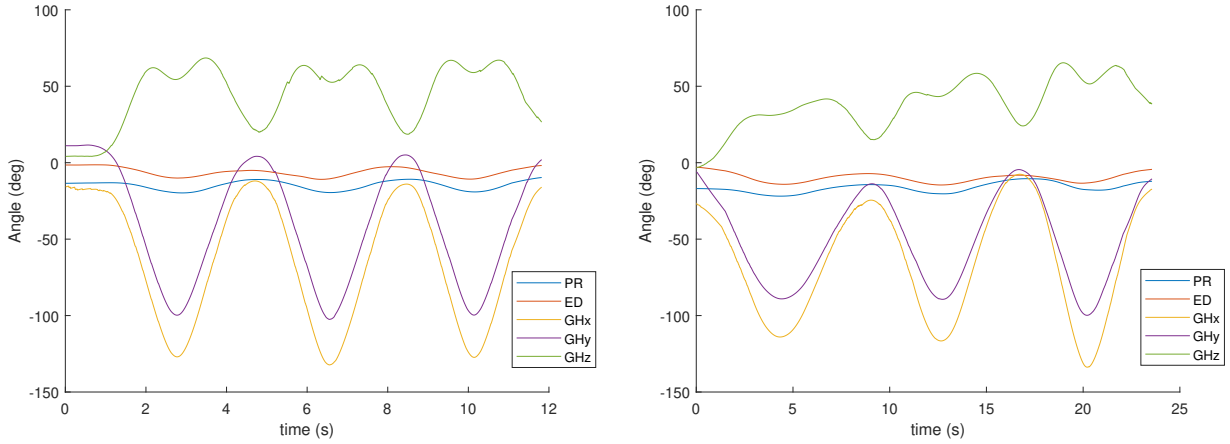

(a) Scapular flexion - fast trial

(b) Scapular flexion - slow trial

Figure 3.4: Full 5 DOFs angle trajectories for experimental scapular flexion data collected by Bosterlee et al [2]

3.4.1 3 DOFs Model

Figure 3.5 shows the results obtained using the 3 DOFs model with the elbow position expressed with respect to the GH joint for one repetition of the movement during both slow and fast trials collected by [2]. Figure 3.5(a) shows the abduction range of motion in the frontal YZ plane during both fast and slow trials. Figure 3.5(b) shows the elbow's trajectory during the fast and slow full range of motion trials for sagittal flexion in the saggital XY plane. Finally, since scapular flexion occurs in the plane 45 degrees between the sagittal and frontal planes, the elbow's trajectory in both of these planes during both fast and slow full ROM trials is shown in Figure 3.5(c) with frontal YZ on the left and sagittal XY on the right.

Based on Figure 3.5, the motion is roughly symmetric with respect to the phase of movement of the arm away from the body and the phase of the movement of the arm returning towards the body. Therefore, in order to decrease the number of data points for optimization, only the "away" phase will be considered throughout the remainder of this

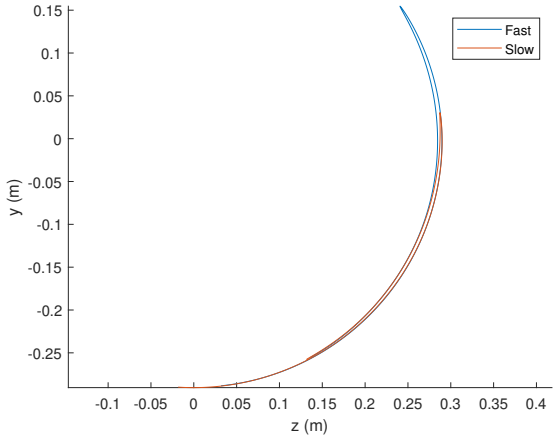

(a) Abduction

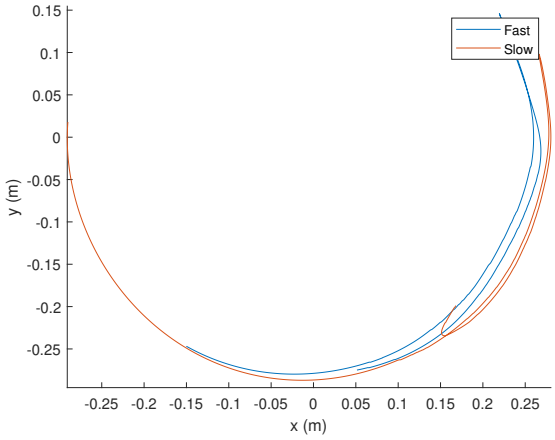

(b) Sagittal Flexion

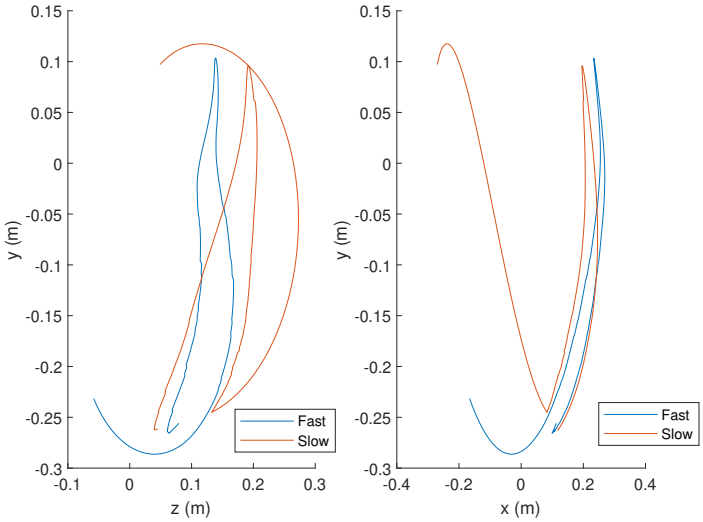

(c) Scapular Flexion

Figure 3.5: Elbow Trajectory in the Human CS During Full ROM Abduction, Sagittal Flexion, and Scapular Flexion (3 DOFs Model)

thesis. Additionally, since fast and slow trials yielded similar results in range of motion, it was decided to focus on only the fast trials for the remainder of the thesis.

The timestamp of the data segments extracted from the full motion capture trajectories presented in Figures 3.2-3.4 are provided in Table 3.2.

Table 3.2: Trial start and end times

Movement	Start time (s)	End time (s)
Abduction	0.77	3.17
Sagittal Flexion	1.71	4.72
Scapular Flexion	1.19	2.69

3.4.2 5 DOFs Model

Elbow Trajectory With Respect to SC

The data set was also examined using the 5 DOFs model to see the effect of the SC joint movement on the overall trajectory of the elbow. The simulation using the 5 DOFs model outputted the elbow trajectory from the SC joint to the elbow joint. For fair comparison, the data obtained from the 3 DOFs model of GH motion was transformed such that the position of the elbow is expressed with respect to the SC joint, rather than the GH joint, assuming a constant value of zero for the SC joint angles.

GH Translation

One assumption of the optimization in Ch. 4 is that the exoskeleton DOFs corresponding to GH movement can be optimized separately from the DOFs corresponding to the translation of the human's GH joint via SC movement. This assumption is valid if the mechanism actuating the other DOFs is able to accurately track the translation of the GH joint and align distal joints of the exoskeleton appropriately. Therefore, this translation of the GH joint with respect to the SC joint during full 5 DOFs shoulder movement was obtained using another Simulink Transform Sensor block. The data was then demeaned by subtracting the average value of each coordinate from the entire trajectory in order to center the data at

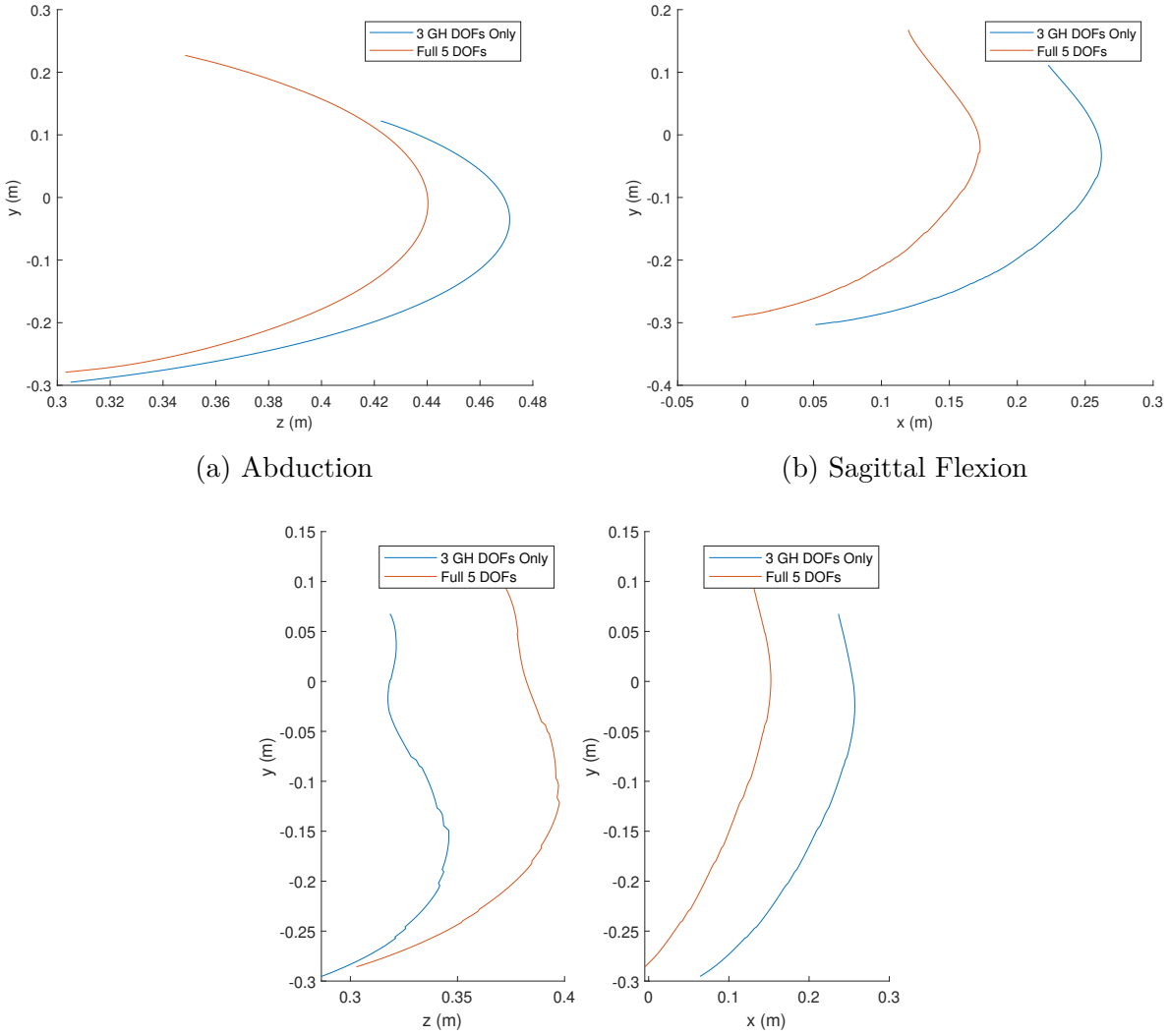

(a) Abduction

(b) Sagittal Flexion

(c) Scapular Flexion

Figure 3.6: Elbow Trajectory in the Human CS During Full ROM Abduction, Sagittal Flexion, and Scapular Flexion (Comparison of 3 and 5 DOFs Models)

$\{0, 0, 0\}$ of a local GH coordinate system. The demeaned data for each of the trajectories is shown in Figure 3.7. Based on these results, the translation of the GH joint makes a more significant difference to the overall motion in the abduction case compared to sagittal and scapular flexion.

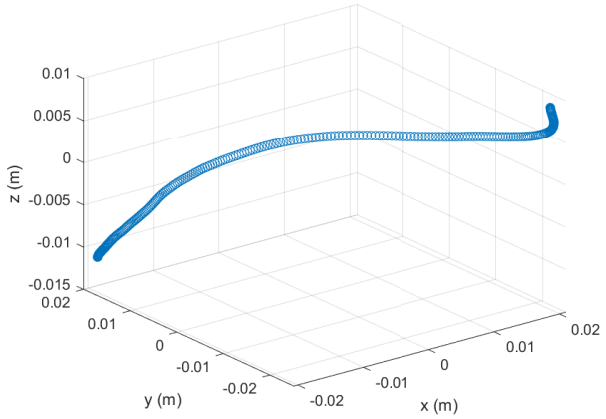

(a) Abduction

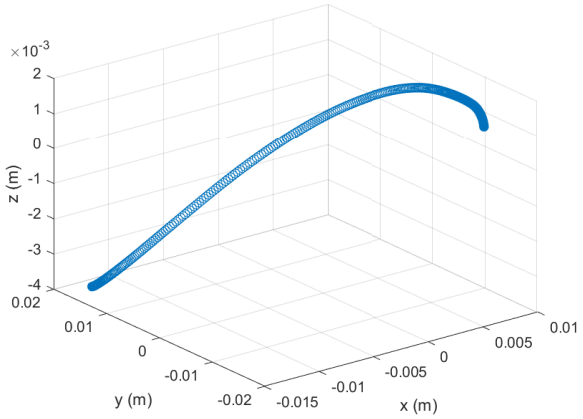

(b) Sagittal Flexion

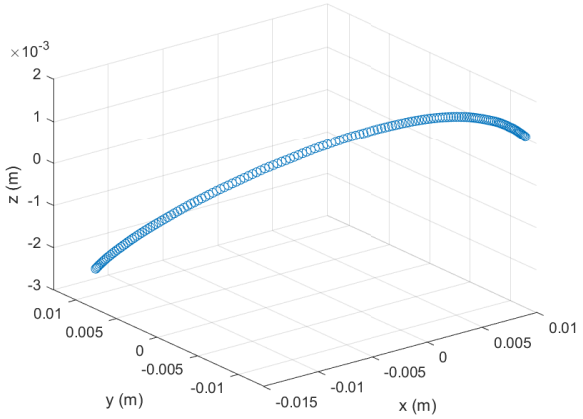

(c) Scapular Flexion

Figure 3.7: Translated GH Trajectory

3.4.3 Conversion of Coordinate Systems

In order for the human kinematics to be compatible with the exoskeleton, the following rotation matrix, R_{HE}, is required to convert the elbow position in the human coordinate system to the position in the robot coordinate system, described in Ch. 2.2.

$$R_{\mathrm{HE}} = \begin{bmatrix} 0 & 0 & 1 \\ 1 & 0 & 0 \\ 0 & 1 & 0 \end{bmatrix} \tag{3.6}$$

Overall, this chapter has provided an overview of the motion capture work done by Bosterlee et al [2] and the processing of abduction, sagittal flexion, and scapular flexion trials. The experimental angle results for each of the five relevant DOF of the shoulder are computed during each trial. A comparison of the forward kinematics using these angles to determine the elbow's trajectory showed a significant difference between 3 and 5 DOFs models. Therefore, it is clear that the translation of the GH joint cannot be ignored when considering the full motion of the shoulder girdle. The next chapter primarily utilizes 3 DOFs data described in this chapter to perform optimization of the 3 DOFs exoskeleton. Full use of the 5 DOFs data will be saved for future work.

Chapter 4

Optimization

The goal of the optimization problem is to choose exoskeleton link lengths to maximize the overlap between the exoskeleton's reachable workspace and the desired human workspace computed using the experimental data in Ch 3. This chapter explains the relevant components of the problem setup including the cost function, desired workspace, bounds, and constraints. The Matlab code implementing this optimization algorithm can be found in the appendix.

4.1 Problem Setup

Since the optimization problem is nonlinear and constrained, Matlab's fmincon function was chosen as an appropriate solver. In general, fmincon solves an optimization problems specified by

$$min f(x) \text{ such that : } \begin{cases} lb \leq x \leq ub \\ c(x) \leq 0 \\ c_{eq}(x) = 0 \\ A\ x \leq b \\ A_{eq}\ x = b_{eq} \end{cases}, \tag{4.1}$$

where $f(x)$ is the cost function, x is a vector of design variables, lb and ub are lower and upper bounds respectively, $c(x)$ and $c_{eq}(x)$ are functions returning nonlinear inequality and equality constraints, and $A\ x \leq b$ and $A_{eq}\ x = b_{eq}$ are linear inequality and equality constraints. In the case of this optimization problem, there are no linear or nonlinear equality constraints. The relevant components are discussed in further detail in the remainder of this chapter.

4.1.1 Cost Function

The cost function is a function of the optimization variables, x, and the desired workspace. For each data point in the desired workspace, the procedure outlined in Algorithm 6 is performed. First, inverse kinematics, as described in Ch. 2.2.2, is used to compute the set of exoskeleton joint angles, Q, to reach the desired end effector position. The initial guess provided to ode15s was chosen to be the angles Q calculated at the previous timestep. The next step in the procedure is to compute forward kinematics, also described in Ch. 2.2.2, to compute the position that the end effector of the exoskeleton is actually able to achieve. There may be configurations the exoskeleton could not reach given the current link lengths, in which case the solver could fail to find reasonable solution, or the numerical methods could produce error. Therefore, the error distance between the desired and actual positions is a reasonable estimate of whether a given point in the desired workspace is achievable. The output of the cost function is the maximum error between the actual position of the exoskeleton, x, y, z, and the desired position, $x_{\text{des}}, y_{\text{des}}, z_{\text{des}}$ over the entire dataset of N desired end effector positions shown by

$$\text{cost} = \max_{i=1\ldots N} \sqrt{(x_{\text{des}} - x_i)^2 + (y_{\text{des}} - y_i)^2 + (z_{\text{des}} - z_i)^2}. \tag{4.2}$$

Desired workspace

As mentioned in Chapter 3, the motions of interest were abduction, sagittal plane flexion, and scapular plane flexion. As detailed in Ch. 3, the experimental data collected by [2] was used to examine full ROM trials of the three movements. In order to reduce the overall number of data points to feed into the optimization algorithm, it was chosen to focus on the upward phase of the trial only, assuming that the downward phase is symmetric. The XZY Euler angles describing the GH rotations required to produce the movement captured

Algorithm 6 Optimization Cost Function

function COST(x, elbow_position)

max_dist = 0

for i = 1, 2,... # data points in elbow_position **do**

Desired position $\{x_{\text{des}}, y_{\text{des}}, z_{\text{des}}\}$ = elbow_position(i)

IK to calculate Q:
$Q = ode15s(\text{InverseKinematics}, 0 : timestep : t_{final}, Q(i-1))$

FK to calculate actual exoskeleton position $\{x, y, z\}$ given Q: $T_{03} = T_{01}T_{12}T_{13}$
$\{x, y, z\} = T_{03}(1:3, 4)$

Distance between actual and desired:
$dist_i = \sqrt{(x_{\text{des}} - x_i)^2 + (y_{\text{des}} - y_i)^2 + (z_{\text{des}} - z_i)^2}$

if $dist_i > max\_dist$ **then**
Update value: $max\_dist = dist_i$
end if

end for
cost = max_dist
Return cost

end function

by the raw marker data were computed using the methods described in Ch. 3.3.2 and can be seen in Figures 3.2-4. These angles were then used as inputs of the human Simulink model developed in Ch. 2.1 to output the end effector forward kinematics. The resulting trajectories of the elbow represent the desired workspace and are combined into a matrix form to be inputted into the cost function. In addition to optimizing link lengths to match the full trajectory of experimental data points across all three motions, the three individual trial trajectories were optimized separately for comparison, described further in Ch. 5.

4.1.2 Optimization Variables

The optimization variables, x, expressed by a 6x1 vector, represent the design variables of the exoskeleton to be optimized. As detailed in Ch. 2.2, the variables to be optimize include the distance from θ_1 to the human user's GH joint ($L_{\text{GH},5}$) and the link lengths L_0 L_1, L_2, L_3, and L_4. These parameters are shown in Figures 2.3 and 2.5.

4.1.3 Bounds

To constrain the optimization problem, lower and upper bounds are given to each optimization variable. For the lower bounds, each dimension must be greater or equal to zero, since these quantities represent physical lengths.

$L_{\text{GH},5}$ is the most anthropometrically valuable design variable, representing the distance between the exoskeleton and the human. This quantity depends on the size of the human to avoid collision between the exoskeleton and user. Therefore, a distance of 0.05 m was used as a lower bound. In order to determine realistic bounds for the rest of the design variables, a 3D-printed prototype was developed based on the design of the Harmony exoskeleton [6], which used 60 degree angles between joint axes.

Empirical kinematic studies using this prototype were performed to estimate approximate link lengths to fit an average human, resulting in the lower bounds for each variable listed in Table 4.1. The prototype could also provide intuitive estimates for upper bounds, however the upper bounds were instead chosen arbitrarily to be 1 m to be an overestimate of the link length requirements.

Table 4.1: Design Variable Bounds

Variable	Lower Bound (m)	Upper Bound (m)
L_0	0	1
L_1	0.05	1
L_2	0.06	1
L_3	0.1	1
L_4	0.05	1
$L_{\mathrm{GH},5}$	0.05	1

4.1.4 Initial Guess

Since optimization is an iterative process, it is important to provide the algorithm with a reasonable starting point. The initial guess of the optimization variables, shown in Table 4.2, was chosen based on the dimensions of the 3D printed prototype and adjusted through trial and error to be values that satisfy all of the constraints presented in the next section.

4.1.5 Nonlinear Constraints

In order to prevent the exoskeleton from interfering with the human, it is mandatory that L_{GH}, the distance from each exoskeleton joint to the human GH joint, is greater than zero, or some value related to the user's anthropometry. The lower bound of $L_{\mathrm{GH},5}$ (0.05 m in

Table 4.2: Initial Guess

Variable	Initial Guess (m)
L_0	0.20
L_1	0.09
L_2	0.07
L_3	0.11
L_4	0.07
$L_{\mathrm{GH},5}$	0.14

Table 4.1), was used as the minimum distance and the resulting constraint equations for $L_{\mathrm{GH},1}$, $L_{\mathrm{GH},2}$, $L_{\mathrm{GH},3}$, and $L_{\mathrm{GH},4}$, written in the form of $c(x) \leq 0$ are

$$c_1(x) = 0.05^2 - L_{\mathrm{GH}}^2 - L_4^2, \tag{4.3}$$

$$c_2(x) = 0.05^2 - L_{\mathrm{GH}}^2 - L_4^2 + L_3^2, \tag{4.4}$$

$$c_3(x) = 0.05^2 - L_{\mathrm{GH}}^2 - L_4^2 + L_3^2 - L_2^2, \tag{4.5}$$

$$c_4(x) = 0.05^2 - L_{\mathrm{GH}}^2 - L_4^2 + L_3^2 - L_2^2 + L_1^2. \tag{4.6}$$

4.1.6 Linear Constraints

To make sure that the exoskeleton dimensions are feasible to build, a linear constraint of the form $Ax \leq b$ is required to limit the overall length of the exoskeleton. Choosing A to be a vector of ones, the sum of the link lengths must be equal to or less than some heuristic

value, b. A value of $b = 1$ m was chosen as the heuristic for all simulations. A smaller overall exoskeleton is more feasible to build and results in faster optimization run time since the search space is more constrained. However, caution must be used when modifying the value of b because a smaller value of b also increases the risk of the exoskeleton interfering and colliding with the human user. Future work could also consider changing the weighting of the contribution of various links to the overall length by modifying the A vector. Additionally, instead of one constraint limiting overall length, multiple constraints limiting the lengths of individual bodies could be used.

Chapter 5

Results and Conclusions

This chapter summarizes the results of the modeling and experimental data collection of human shoulder motion from Ch. 2 and 3. This chapter also elaborates upon the results obtained via the algorithm presented in Ch. 4 to optimize the link lengths of the exoskeleton model developed in Ch. 3. Finally, this chapter also includes suggestions for future work expanding the model to additional degrees of freedom and other improvements.

5.1 Results

5.1.1 Shoulder Capabilities Results

A large component of this thesis was devoted to developing a deeper understanding of the movement capabilities of the human shoulder. In Ch. 2, a 3 DOFs model of the GH joint of the shoulder was developed in addition to a 5 DOFs model incorporating the translation of the GH due to movement of the SC joint. Using these models and the experimental data collected by Bolsterlee et al. [2], the angle trajectories of each DOF were computed. The motions studied were abduction, sagittal plane flexion, and scapular flexion during full range of motion trials. The peak values of each DOF, corresponding to the data presented in Figures 3.2-4 are listed in Tables 5.1 and 5.2. This data provides insight to the capabilities of the human during three common movements performed over a full range of motion to

help appropriately determine the requirements to design the exoskeleton's properties and capabilities. From Table 5.1, it is clear that the two degrees of freedom that have the

Table 5.1: GH DOFs Angle Ranges

Movement	GHx (degrees)	GHy (degrees)	GHz (degrees)
Abduction	-123 to -25	-96 to -26	3 to 13
Sagittal Flexion	-149 to -13	-132 to 7	17 to 75
Scapular Flexion	-127 to -7	-99 to 4	12 to 68

Table 5.2: SC DOFs Angle Ranges

Movement	PR (degrees)	ED (degrees)
Abduction	-35 to -15	-20 to 0
Sagittal Flexion	-10 to 0	-20 to -7
Scapular Flexion	-20 to -15	-15 to 0

greatest contribution and largest range of motion across all movements are GHx and GHy. The movement of the SC occurs at a smaller range than the GH joint, but the SC movement still contributes significantly to the overall trajectory of the end effector and cannot be ignored.

5.1.2 Optimization Results

A total of four cases were used to compare optimization results: an abduction trajectory, a sagittal flexion trajectory, a scapular flexion trajectory, and a full trajectory consisting of all all three movements. The simulations in this section were performed using the 3 DOFs motion of the GH joint, omitting the translation of the GH joint due to SC movement. The simulations using the full 5 DOFs human movement are included later in Ch. 5.2.2.

Abduction

Figure 5.1 shows the optimized link lengths for the abduction only trajectory. The angles between joint axes, α_1 and α_2 were 48.21 and 73.78 degrees, respectively. Unlike the Harmony exoskeleton [6], which implemented equal values of 60 degrees for both α_1 and α_2, this trial suggests that α_2 should be greater than α_1, a trend consistent with in the other results presented in later sections. The maximum error distance between the desired and actual positions of the exoskeleton end effector, computed by the cost function described in Ch. 4.1.1, was 0.000134 m for these link lengths. While this is the smallest cost function of all of the cases examined, the abduction-based exoskeleton performs poorly during other movements and is not the best choice overall.

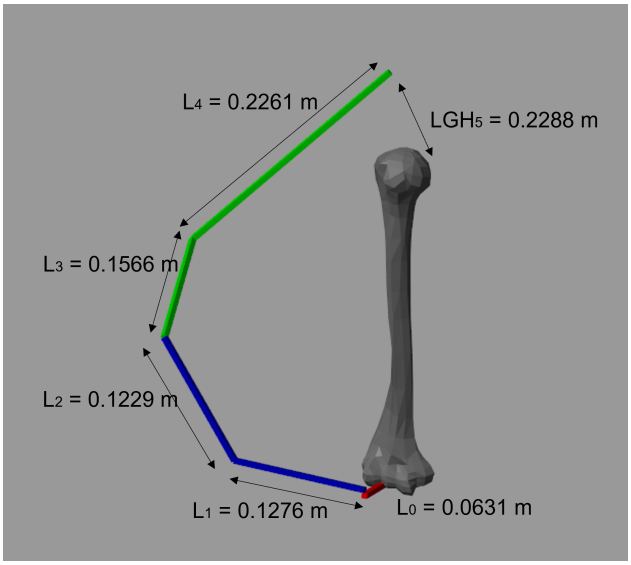

Figure 5.1: Optimized Exoskeleton Link Lengths - Abduction Only

Sagittal Flexion

Figure 5.2 shows the optimized link lengths for the sagittal flexion only trajectory. The angles between joint axes, α_1 and α_2, were 50.24 and 88.27 degrees, respectively. The

maximum error distance between the desired and actual positions of the exoskeleton end effector was 0.0045m for these link lengths. One possible reason for this larger cost compared to the abduction trajectory case is that the sagittal flexion trajectory was more noisy and deviated more from an idealized, symmetric curve curve. However, unlike the exoskeleton dimensions optimized for abduction, the sagittal flexion exoskeleton had consistent error distance performance when tested with other movements in the desired workspace outside of the sagittal flexion trajectory used during optimization.

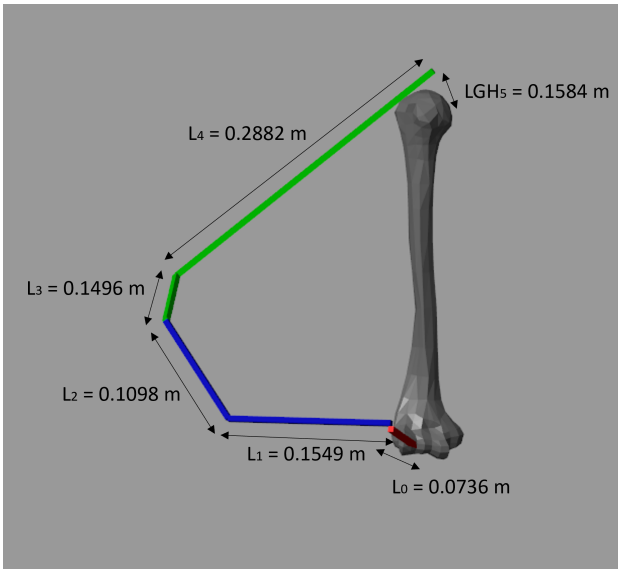

Figure 5.2: Optimized Exoskeleton Link Lengths - Sagittal Flexion Only

Scapular Flexion

Figure 5.3 shows the optimized link lengths for the scapular flexion only trajectory. These lengths and the angles between joint axes, α_1 (85.58 degrees) and α_2 (73.43 degrees) were similar to that of the sagittal flexion exoskeleton. Additionally, the maximum error distance between the desired and actual positions of the exoskeleton end effector was 0.0070 m, similar to that of the sagittal flexion exoskeleton. This exoskeleton also performed consistently for other movements in the desired workspace outside of the scapular flexion trajectory used

during optimization.

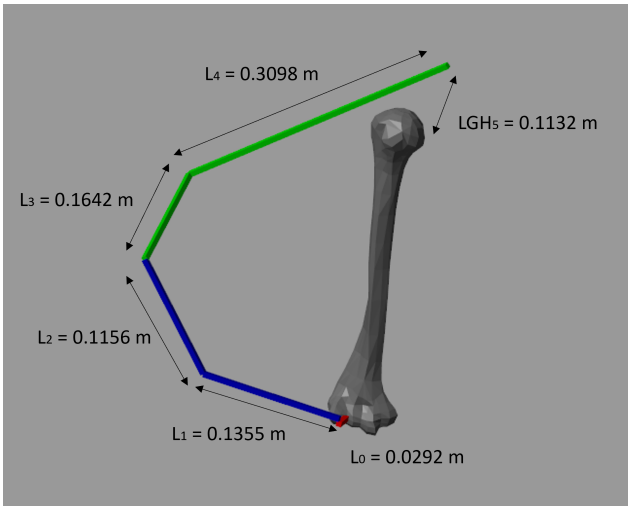

Figure 5.3: Optimized Exoskeleton Link Lengths - Scapular Flexion Only

Full Trajectory

The final case examined was the full trajectory, consisting of the combined matrix of the data points from the abduction, sagittal flexion, and scapular flexion trajectories. Figure 5.4 shows the values of the optimized link lengths. The angles between joint axes, α_1 and α_2, were 51.38 and 91.53 degrees, respectively. With the largest and most spread out trajectory, it was expected that this trajectory would have the highest cost, but this exoskeleton outperforms both sagittal and scapular flexion exoskeletons overall with a cost value of 0.000288 m.

Summary of all 4 cases

The optimized link lengths for all four cases studied are provided in Table 5.3.

Table 5.3 shows the values of α_1 and α_2, which represent the angles between the joint axes, across all cases. In the literature, the Harmony exo [6] uses a value of 60 degrees for

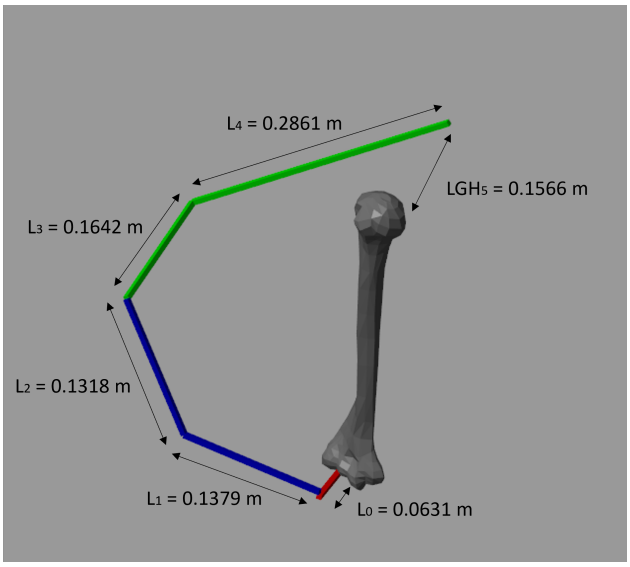

Figure 5.4: Optimized Exoskeleton Link Lengths - Full Trajectory

Table 5.3: Summary of link length results across all 4 cases

Variable	Abduction	Sagittal Flexion	Scapular Flexion	Full Trajectory
L_0 (m)	0.0631	0.0736	0.0292	0.0631
L_1 (m)	0.1276	0.1549	0.1355	0.1379
L_2 (m)	0.1229	0.1098	0.1156	0.1318
L_3 (m)	0.1566	0.1496	0.1642	0.1642
L_4 (m)	0.2261	0.2882	0.3098	0.2861
$L_{\mathrm{GH},5}$ (m)	0.2288	0.1584	0.1132	0.1566

both α_1 and α_2, but this study determined that the the optimal values of these parameters depends on the task. During all cases, the value of α_1 was greater than the value of α_2.

Table 5.4 compares the cost function values for each trajectory, which represents the maximum error distance between actual and desired positions of the end effector over the given trajectory, as explained in Ch. 4.1.1. Figure 5.5 compares the distance error at every timestep throughout the full trajectory of all three movements with regions shaded according to movement. The exoskeleton with the lowest maximum cost during its optimized trajectory

Table 5.4: Summary of α_1, and α_2 across all 4 cases

Variable	Abduction	Sagittal Flexion	Scapular Flexion	Full Trajectory
α_1 (degrees)	48.21	50.24	48.05	51.38
α_2 (degrees)	73.78	88.27	99.79	91.53

Table 5.5: Summary of cost function and error across all 4 cases

Variable	Abduction	Sagittal Flexion	Scapular Flexion	Full Trajectory
Cost (m)	0.000134	0.0045	0.0070	0.000288

was the abduction-based exoskeleton, but as shown in Figure 5.5, this exoskeleton performs the worst overall during movements outside of its optimized trajectory. Errors up to 0.3 m are present as the arm moves away from the body in the mid to upper ranges of flexion movements. The error distances for the sagittal and scapular flexion and full trajectory exoskeletons are constant. Of all of the cases studied, the exoskeleton optimized using the full trajectory provides the best performance.

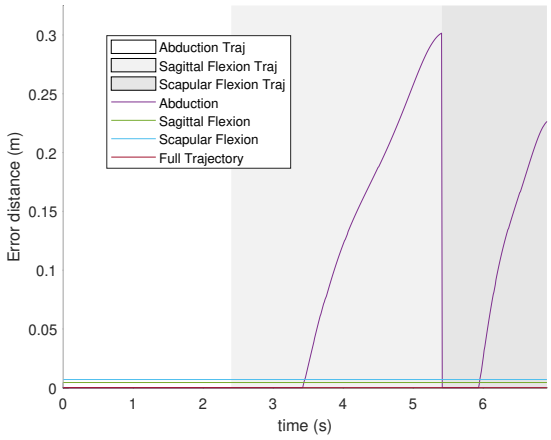

Figure 5.5: Error distances for 4 cases over the full trajectory

5.2 Additional Simulations

5.2.1 2 DOFs Model

One observation from the previous simulations is that L_0 is consistently shorter than the other link lengths across all cases, prompting the question of if this link is truly necessary to achieve the desired workspace. Therefore, the simulation was run again using the full trajectory of all three motions and an increased b value of 1.1 m to ensure convergence. L_0 was constrained to be 0 m, effectively eliminating the third degree of freedom, by setting both the lower and upper bounds of the variable to be 0 m. The resulting values of the other design variables are shown in Table 5.6. Compared to the results of previous simulations, the value of $L_{\text{GH},5}$ is significantly larger for this 2 DOFs model. Figure 5.6 shows the distance error for this exoskeleton design using the same methods used in Figure 5.5. The error is several orders of magnitude greater than that of the errors achieved during the 3 DOFs simulations. Another disadvantage of this 2 DOFs model is the decrease in overall DOFs, which would negatively affect the workspace outside of the tested motion trajectories. Clearly, the third DOF is necessary to fully capture the movement of the shoulder as related to the 3 DOFs GH joint.

Table 5.6: Link length results for the $L_0 = 0$ case

Variable	Length (m)
L_0 (m)	0.0000
L_1 (m)	0.1871
L_2 (m)	0.1080
L_3 (m)	0.1987
L_4 (m)	0.1592
$L_{\text{GH},5}$ (m)	0.4688

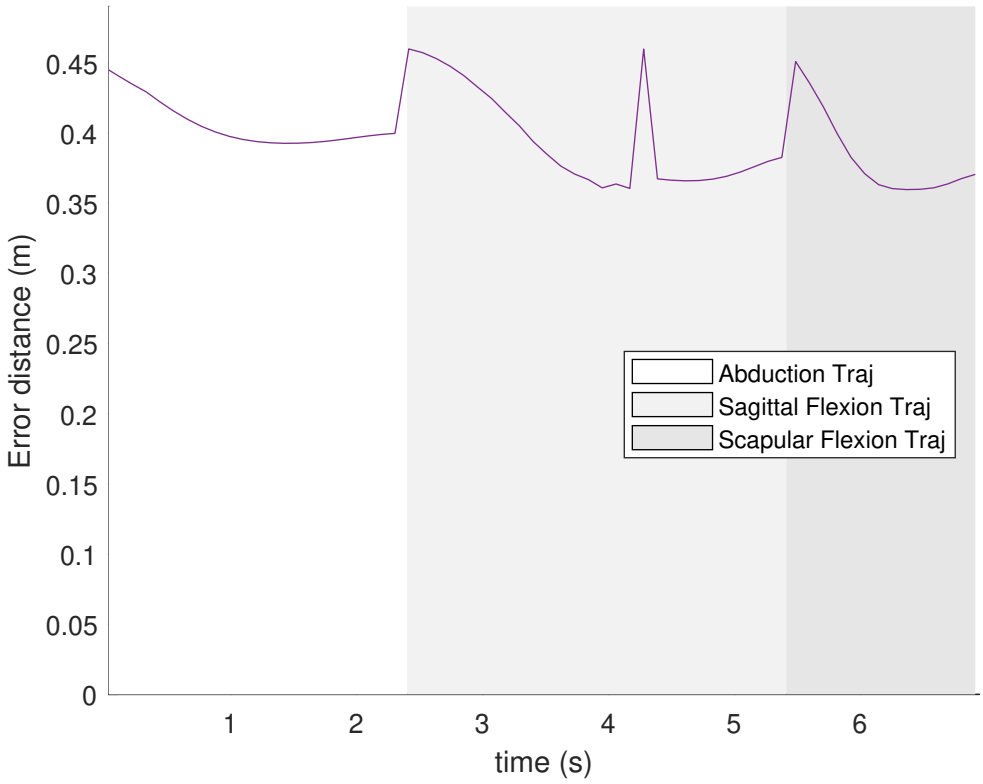

Figure 5.6: Error distances for the $L_0 = 0$ case

5.2.2 5 DOFs Movement

Validation using 5 DOFs trajectory

A main assumption throughout the optimization was that the distal links of the exoskeleton could be optimized according to pure GH motion if a mechanism, also optimized separately, was developed in future studies that ensured proper tracking and alignment of the human's GH joint and these distal links with respect to a constant offset, $L_{\mathrm{GH},5}$. Therefore, optimization was performed using the trajectories produced using the 3 DOFs human shoulder model, assuming no translation of the GH. The purpose of this section is to determine the robustness of the optimized link lengths from the 3 DOFs simulation with respect to the full

5 DOFs motion. This was done by computing the translation of the GH joint due to SC joint movement and translating the trajectory to represent it in a local frame, as shown previously in Figure 3.7. The desired elbow position, used during forward dynamics, was modified by adding this $\{x, y, z\}$ GH translation offset to the original elbow position vector. The same cost function minimizing the distance between the desired and achieved end effector positions was used with this modified desired trajectory representing the full 5 DOFs motion. Using the optimized link lengths from the best 3 DOFs simulation (case 4 – full trajectory), the error distances are presented in Figure 5.7. While the errors are larger than the case where the GH was stationary, the maximum distance error across the full trajectory was roughly 2.5 cm, suggesting that the optimized link lengths are robust enough to handle deviations in alignment between the exo and GH joint if the additional two DOFs to accommodate translation were not incorporated.

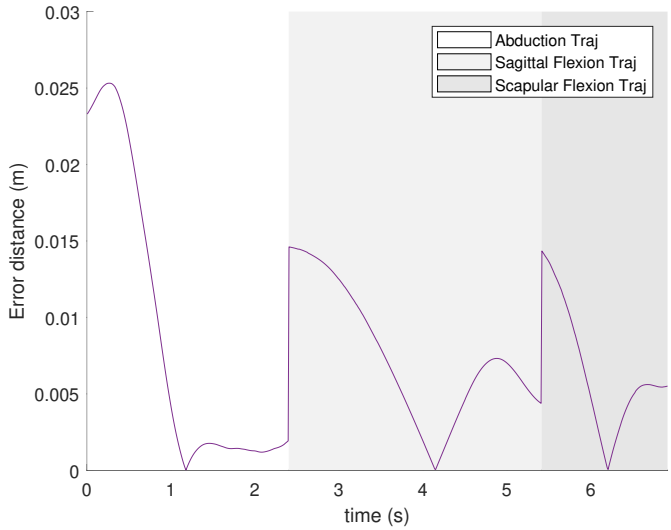

Figure 5.7: Error distances for translating GH trajectory

Optimization using 5 DOFs trajectory

The optimization algorithm was re-run using the modified 5 DOFs trajectory incorporating the translation of the GH joint while still using the 3 DOFs exoskeleton model aligning with $\{0, 0, 0\}$ of the de-meaned GH translation. Using the same cost function, the maximum error distance for the optimized link lengths, listed in Table 5.7, was 0.0163 m, which is comparable to the results of the previous simulation testing the exoskeleton optimized for 3 DOFs motion with the full 5 DOFs data.

Table 5.7: Link length results optimized using 5 DOFs data

Variable	Length (m)
L_0 (m)	0.0793
L_1 (m)	0.1309
L_2 (m)	0.1238
L_3 (m)	0.1541
L_4 (m)	0.2868
$L_{\mathrm{GH},5}$ (m)	0.1552

5.3 Final Recommendations

The simulation testing a 2 DOFs model omitting the L_0 link (Ch. 5.2.1), resulted in significantly higher errors than the full 3 DOFs model in terms of replicating the workspace of the three shoulder movements studied in this thesis. Therefore, it is clear that a minimum of 3 DOFs is required to represent GH movement. Simulations with a 3 DOFs exoskeleton and 3 DOFs human GH motion data yielded similar results when optimized based on abduction, sagittal flexion, scapular flexion, and the full trajectory, with the results from optimizing with the full trajectory providing the lowest overall error. Based on these results, the link lengths presented in Figure 5.4 are recommended for implementation in the system. The

cost function was evaluated using these link lengths and a modified elbow position trajectory incorporating the translation of the GH joint due to the other DOFs of the shoulder girdle, as seen in the previous subsection, yielding errors below 2.5 cm. While the optimized link length values create an exoskeleton that is robust in regards to such misalignments between human and exoskeleton, it is recommended that more work to expand the exoskeleton to 5 DOFs is needed. The 3 DOFs exoskeleton parameters optimized using the full 5 DOFs human data performed similarly to the exoskeleton optimized based on 3 DOFs data, with a maximum error of 1.6 cm. A 5 DOFs exoskeleton will likely improve on the results of the presented 3 DOFs exoskeleton and ensure greater kinematic compatibility between human and exoskeleton, increasing user safety.

5.4 Future Work

DOF

The work presented in this thesis was conducted under the assumption that the 3 rotational DOFs of the GH joint and the 2 translational DOFs of the shoulder girdle could be considered separately. Optimization of a 3 DOFs exoskeleton could be performed separately, assuming that additional DOFs would allow the alignment and tracking of the human's GH joint. This idea was validated by the work in the previous section testing the full 5 DOFs movement using the exoskeleton link lengths optimized using three DOFs. In the future, a similar optimization procedure should be completed considering the GH as the end effector and optimizing to match the exo's workspace with the translation movement of the GH joint of the human.

Collision and Singularity Avoidance

Another future improvement of this work would be the incorporation of more robust collision detection and avoidance. Robot interference with the human could significantly impact user safety. Forward kinematic analysis should be conducted for each joint of the exoskeleton throughout the desired trajectory and compared to an estimate of the location of the human at each timestep. Tuning of the linear constraint heuristic discussed in Ch. 4.1.6 that limits the overall length of the exoskeleton is also an important consideration in collision avoidance.

Singularities in the robot's workspace could also cause limitations in reaching the desired workspace. A singularity occurs when the robot reaches a configuration where one or more degrees of freedom are lost. By including manipulability, a measure of how close the determinant of the Jacobian is to reaching a singular value of 0, into the cost function of the optimization, the effect of singularities could be reduced. The equation to compute manipulability, M, is

$$M = \sqrt{JJ^T}, \tag{5.1}$$

where J is the Jacobian and J^T is its transpose.

Experimental Data Collection

Future work could also include the in-house collection of motion capture data. Since the exoskeleton is intended to serve as an emulator to examine a wide variety of applications and control strategies, the full range of motion data sets captured by [2] served as an acceptable baseline. However, if more specific uses of the exoskeleton were determined, motion capture

involving application-specific movements could provide a more accurate estimate of the target human workspace, which would affect the optimization results. Additionally, the comparison across multiple subjects of varying anthropometry and multiple trials of the same movement could provide a more broad understanding of shoulder capabilities to allow the exoskeleton to be adaptable for different users.

Bibliography

[1] M. N. Castro, J. Rasmussen, M. S. Andersen, and S. Bai, "A compact 3-DOF shoulder mechanism constructed with scissors linkages for exoskeleton applications," vol. 132, pp. 264–278.

[2] B. Bolsterlee, H. E. J. Veeger, and F. C. T. van der Helm, "Modelling clavicular and scapular kinematics: from measurement to simulation," vol. 52, no. 3, pp. 283–291.

[3] D. B. Chaffin, G. B. J. Andersson, and B. J. Martin, *Occupational Biomechanics*. John Wiley & Sons, Inc., 4th ed., 2006.

[4] S. J. Ball, I. Brown, and S. H. Scott, "Designing a robotic exoskeleton for shoulder complex rehabilitation," vol. 30.

[5] S. J. Ball, I. E. Brown, and S. H. Scott, "MEDARM: a rehabilitation robot with 5dof at the shoulder complex," in *2007 IEEE/ASME international conference on advanced intelligent mechatronics*, pp. 1–6. ISSN: 2159-6255.

[6] B. Kim and A. D. Deshpande, "An upper-body rehabilitation exoskeleton harmony with an anatomical shoulder mechanism: Design, modeling, control, and performance evaluation," vol. 36, no. 4, pp. 414–435. Publisher: SAGE Publications Ltd STM.

[7] J. Narayan, B. Kalita, and S. K. Dwivedy, "Development of robot-based upper limb devices for rehabilitation purposes: a systematic review," vol. 6, no. 1, p. 4.

[8] P. M. Kuber, M. Abdollahi, M. M. Alemi, and E. Rashedi, "A systematic review on evaluation strategies for field assessment of upper-body industrial exoskeletons: Current practices and future trends," vol. 50, no. 10, pp. 1203–1231.

[9] J. Yoon, S. Kim, J. Moon, J. Kim, and G. Lee, "Minimizing misalignment and frame protrusion of shoulder exoskeleton via optimization for reducing interaction force and minimizing volume," vol. 10, no. 12, p. 1223. Number: 12 Publisher: Multidisciplinary Digital Publishing Institute.

[10] A. Schiele and F. C. T. van der Helm, "Kinematic design to improve ergonomics in human machine interaction," vol. 14, no. 4, pp. 456–469. Conference Name: IEEE Transactions on Neural Systems and Rehabilitation Engineering.

[11] G. Wu, F. C. T. van der Helm, H. E. J. (DirkJan) Veeger, M. Makhsous, P. Van Roy, C. Anglin, J. Nagels, A. R. Karduna, K. McQuade, X. Wang, F. W. Werner, and B. Buchholz, "ISB recommendation on definitions of joint coordinate systems of various joints for the reporting of human joint motion—part II: shoulder, elbow, wrist and hand," vol. 38, no. 5, pp. 981–992.

[12] V. Phadke, J. P. Braman, R. F. LaPrade, and P. M. Ludewig, "Comparison of glenohumeral motion using different rotation sequences," vol. 44, no. 4, pp. 700–705.

[13] F. C. van der Helm, "A finite element musculoskeletal model of the shoulder mechanism," vol. 27, no. 5, pp. 551–569.

[14] A. Sodemann, "Robotics 1 u1 (kinematics) s5 (htm) p2 (htm by denavit hartenberg)," Sept. 2017.

[15] A. A. Nikooyan, F. C. T. van der Helm, P. Westerhoff, F. Graichen, G. Bergmann, and H. E. J. D. Veeger, "Comparison of two methods for in vivo estimation of the glenohumeral joint rotation center (GH-JRC) of the patients with shoulder hemiarthroplasty," vol. 6, no. 3, p. e18488.

Appendices

Appendix A

A.1 Derivations

Table 2.2 in the main text lists the DH parameters comprising the model of the exoskeleton. The variables are shown in Figures 2.3 and 2.5 and the equations describing the geometric and trigonometric relationships to derive these variables are shown in the following equations

$$L_{\mathrm{GH},4} = \sqrt{L_{\mathrm{GH},5}^2 + L_4^2}, \tag{A.1}$$

$$L_{\mathrm{GH},3} = \sqrt{L_{\mathrm{GH},4}^2 - L_3^2}, \tag{A.2}$$

$$L_{\mathrm{GH},2} = \sqrt{L_{\mathrm{GH},3}^2 + L_2^2}, \tag{A.3}$$

$$L_{\mathrm{GH},1} = \sqrt{L_{\mathrm{GH},2}^2 - L_1^2} + \mathrm{thickness}, \tag{A.4}$$

$$\alpha_1 = \tan^{-1}(\frac{L_4}{L_{\mathrm{GH},5}}) + \sin(\frac{L_3}{L_{\mathrm{GH},4}}), \tag{A.5}$$

$$\alpha_2 = \tan^{-1}(\frac{L_2}{L_{\mathrm{GH},3}}) + \sin(\frac{L_1}{L_{\mathrm{GH},2}}). \tag{A.6}$$

A.2 Code

A.2.1 Optimization Code

The code used to implement the optimization algorithm described in Ch. 4 to obtain the results presented in Ch. 5 is below.

```
clc,clear,close all

%% Optimization Problem setup
% Linear constraints
A = [1 1 1 1 1 1];
b = 1;
Aeq =[];
beq = [];

% Bounds
lb = [0.05 0.05 0.1 0.06 0.05 0];
ub = [1 1 1 1 1 1];

% Initial guess
x0 = [0.14 0.07 0.11 0.07 0.09 0.2];

% Nonlinear constraints
min_dist = 0.05;
nonlin = @(x)mycon(x,min_dist);

%Output options
options = optimoptions('fmincon','Display','iter','PlotFcn','optimplotx');

%% Load elbow position trajectory
```

```
25 load(fileName);
26
27 %% Run optimization algorithm
28 tic
29 [x_opt,cost] = fmincon(@(x)opt(x,pos_elbow),x0,A,b,Aeq,beq,lb,ub,nonlin,
       options)
30 toc
31
32 %% Output results
33 [Q_opt,pos_exo,dist] = results(x_opt,pos_elbow);
34
35 % Plot distance error over the duration of the trajectory
36 figure
37 plot(dist)
38
39 % Plot elbow position and exo end effector position
40 pos_elbow = pos_elbow + [0;0;x_opt(1)]; %convert human CS to exo CS
41 figure
42 hold on
43 plot3(pos_exo(1,:),pos_exo(2,:),pos_exo(3,:))
44 plot3(pos_elbow(1,:),pos_elbow(2,:),pos_elbow(3,:))
45 legend('exo','elbow')
46 hold off
47
48 %% Functions
49 % Nonlinear constraints
50 function [c,ceq] = mycon(x,min_dist)
51     c(1) = min_dist^2 - x(1)^2 - x(2)^2; %LGH4 > min_dist
52     c(2) = min_dist^2 - x(1)^2 - x(2)^2 + x(3)^2;  %LGH3 > min_dist
53     c(3) = min_dist^2 - x(1)^2 - x(2)^2 + x(3)^2 - x(4)^2; %LGH2 > min_dist
54     c(4) = min_dist^2 - x(1)^2 - x(2)^2 + x(3)^2 - x(4)^2 + x(5)^2; %LGH1 >
```

```
        min_dist

    ceq = [];   % Compute nonlinear equalities at x.
end

% Inverse kinematics
function Q_DOT = numericalIK(t,Q,x,pos_elbow,i)
    % Alpha (step size)
    alpha = 1*eye(3);
    % Compute Jacobian
    J = J_fun(x,Q(1),Q(2),Q(3));
    % Desired X - elbow
    X_des = pos_elbow(:,i)+ [0; 0; x(1)]; % offset of LGH5 in z direction

    % Desired Xdot - zeros
    X_dot_des = [0; 0; 0];

    % Robot pos
    T03 = real(T03_fun(x,Q(1),Q(2),Q(3)));
    RobotPos = T03(1:3,4);

    Q_DOT = pinv(J)*(X_des + alpha*(X_dot_des - RobotPos));

end
function cost = opt(x,pos_elbow)
    pos_elbow_temp = pos_elbow + [0; 0; x(1)];

    % ODE parameters
    t_final = 8;
    timestep = 1;
    th0 = [0; 0; 0];
```

```
85
86      i = 1;
87      % Run 1st iteration outside of loop
88      [~, Q] = ode15s(@(t,Q)numericalIK(t,Q,x,pos_elbow,i),0:timestep:t_final,th0
            );
89      Q_opt(i,:) = real(Q(end,:));
90
91      pos_exo = zeros(3,length(pos_elbow));
92
93      T03 = real(T03_fun(x,Q_opt(i,1),Q_opt(i,2),Q_opt(i,3)));
94      pos_exo(:,i) = T03(1:3,4);
95
96      dist_cost = sqrt((pos_exo(1,i)-pos_elbow_temp(1,i))^2 + (pos_exo(2,i)-
            pos_elbow_temp(2,i))^2 + (pos_exo(3,i)-pos_elbow_temp(3,i))^2);
97
98      for i = 2:length(pos_elbow)
99
100         % 1. Use IK to solve for exo joint values that get it to match the
                desired end
101         % effector position (elbow)
102         [~, Q] = ode15s(@(t,Q)numericalIK(t,Q,x,pos_elbow,i),0:timestep:t_final
                ,Q_opt(i-1,:));
103         Q_opt(i,:) = Q(end,:);
104
105         % 2. Use FK to calculate the XYZ positions of end effector at this
106         % configuration
107         T03 = T03_fun(x,Q_opt(i,1),Q_opt(i,2),Q_opt(i,3));
108         pos_exo(:,i) = T03(1:3,4);
109         % Compute error (distance between desired and achieved positions)
110
111         dist = sqrt((pos_exo(1,i)-pos_elbow_temp(1,i))^2 + (pos_exo(2,i)-
```

```
            pos_elbow_temp(2,i))^2 + (pos_exo(3,i)-pos_elbow_temp(3,i))^2);
        if dist > dist_cost
            dist_cost = dist;
        end
    end

    cost = dist_cost;
end

% Results (very similar to opt function with different outputs)
function [Q_opt,pos_exo,dist] = results(x,pos_elbow)
    pos_elbow_temp = pos_elbow + [0; 0; x(1)];
    % ODE parameters
    t_final = 10;
    timestep = 0.1;
    th0 = [0; 0; 0];

    i = 1;
    % Run 1st iteration outside of loop
    [~, Q] = ode15s(@(t,Q)numericalIK(t,Q,x,pos_elbow,i),0:timestep:t_final,th0
        );
    Q_opt(i,:) = Q(end,:);

    pos_exo = zeros(3,length(pos_elbow));

    T03 = T03_fun(x,Q_opt(i,1),Q_opt(i,2),Q_opt(i,3));
    pos_exo(:,i) = T03(1:3,4);

    dist(i) = sqrt((pos_exo(1,i)-pos_elbow_temp(1,i))^2 + (pos_exo(2,i)-
        pos_elbow_temp(2,i))^2 + (pos_exo(3,i)-pos_elbow_temp(3,i))^2);

```

```
140     for i = 2:length(pos_elbow)
141         % 1. Use IK to solve for exo joint values that get it to match the
                desired end
142         % effector position (elbow)
143         [~, Q] = ode15s(@(t,Q)numericalIK(t,Q,x,pos_elbow,i),0:timestep:t_final
                ,Q_opt(i-1,:));
144         Q_opt(i,:) = Q(end,:);
145
146         % 2. Use FK to calculate the XYZ positions of end effector
147         T03 = T03_fun(x,Q_opt(i,1),Q_opt(i,2),Q_opt(i,3));
148         pos_exo(:,i) = T03(1:3,4);
149
150         % Compute error (distance between desired and achieved positions)
151         dist(i) = sqrt((pos_exo(1,i)-pos_elbow_temp(1,i))^2 + (pos_exo(2,i)-
                pos_elbow_temp(2,i))^2 + (pos_exo(3,i)-pos_elbow_temp(3,i))^2);
152     end
153 end
```